Teleological Role of L-2-Hydroxyglutarate Dehydrogenase in the Kidney

Garrett Brinkley[1], Hyeyoung Nam[1], Eunhee Shim[1*], Richard Kirkman[1], Anirban Kundu[1], Suman Karki[1], Yasaman Heidarian[2], Jason M. Tennessen[2], Juan Liu[3], Jason W. Locasale[3], Tao Guo[4] , Shi Wei[4], Jennifer Gordetsky[5], Teresa L. Johnson-Pais[6], Devin Absher[7], Dinesh Rakheja[8], Anil K. Challa[9], Sunil Sudarshan[1,10]

Departments of [1]Urology, [4]Pathology, and [9]Biology, University of Alabama at Birmingham; [2]Department of Biology, Indiana University, [3]Department of Pharmacology and Cancer Biology, Duke University; [5]Departments of Pathology and Urology, Vanderbilt University Medical Center; [6]Department of Urology, UT Health San Antonio; [7]HudsonAlpha Institute for Biotechnology; [8]Department of Pathology, University of Texas Southwestern Medical Center; [10]Birmingham VA Medical Center; *Currently at Division of Biology and Biological Engineering, Caltech University

Summary Statement: We demonstrate a novel role for L-2-hydroxyglutarate dehydrogenase in the kidney as well as new insight into the mechanisms that regulate expression of this enzyme.

Garrett Brinkley – gbrink@uab.edu - https://orcid.org/0000-0003-2622-3416
Hyeyoung Nam - hyeyoungnam@uabmc.edu -
Eun-hee Shim - eunhee.shim@gmail.com
Richard Kirkman - richardkirkman@uabmc.edu
Anirban Kundu - anirbankundu@uabmc.edu - https://orcid.org/0000-0003-0621-9989
Suman Karki - sumankarki@uabmc.edu
Juan Liu - juan.liu@duke.edu
Yasaman Heidarian – yheidar@iu.edu
Jason M Tennessen – jtenness@indiana.edu - https://orcid.org/0000-0002-3527-5683
Tao Guo - tguo168@gmail.com
Jason Locasale - dr.jason.locasale@gmail.com- https://orcid.org/0000-0002-7766-3502
Jennifer Gordetsky - jennifer.b.gordetsky@vumc.org - https://orcid.org/0000-0002-0745-216
Shi Wei - swei@uabmc.edu
Teresa Johnson-Pais - paist@uthscsa.edu - https://orcid.org/0000-0001-7580-1206
Devin Absher – dabsher@hudsonalpha.org -
Dinesh Rakheja - dinesh.rakheja@utsouthwestern.edu - https://orcid.org/0000-0001-6888-7902
Anil Challa - akchalla@uab.edu - https://orcid.org/0000-0002-3633-3304
Sunil Sudarshan - ssudarshan@uabmc.edu - https://orcid.org/0000-0001-7257-6277

Keywords: L-2-hydroxyglutarate, L-2-Hydroxyglutarate Dehydrogenase, TCA cycle, PPARG coactivator 1-α

Competing interests: The authors declare no competing or financial interests.

Abstract

L-2-hydroxyglutarate (L-2HG) is an oncometabolite found elevated in renal tumors. However, this molecule may have physiologic roles that extend beyond its association with cancer as L-2HG levels are elevated in response to hypoxia and during *Drosophila* larval development. L-2HG is known to be metabolized by L-2HG dehydrogenase (L2HGDH), and loss of L2HGDH leads to elevated L-2HG levels. Despite being highly expressed in the kidney, L2HGDH's role in renal metabolism has not been explored. Here, we report our findings utilizing a novel CRISPR/Cas9 murine knockout model with a specific focus on the role of L2HGDH in the kidney. Histologically, *L2hgdh KO* kidneys have no demonstrable histologic abnormalities. However, GC/MS metabolomics demonstrates significantly reduced levels of the TCA cycle intermediate succinate in multiple tissues. Isotope labeling studies with [U-^{13}C] glucose demonstrate that restoration of L2HGDH in renal cancer cells (which lowers L-2HG) leads to enhanced incorporation of label into TCA cycle intermediates. Subsequent biochemical studies demonstrate that L-2HG can inhibit the TCA cycle enzyme α-ketoglutarate dehydrogenase. Bioinformatic analysis of mRNA expression data from renal tumors demonstrates that L2HGDH is co-expressed with genes encoding TCA cycle enzymes as well as the gene encoding the transcription factor PGC-1α, which is known to regulate mitochondrial metabolism. Restoration of PGC-1α in renal tumor cells results in increased L2HGDH expression with a concomitant reduction if L-2HG levels. Collectively, our studies provide new insight into the physiologic role for L2HGDH as well as mechanisms that promote L-2HG accumulation in disease states.

Introduction

Oncometabolites are small molecules whose levels are found elevated in various malignancies. To date, these molecules include the tricarboxylic acid (TCA) cycle intermediates succinate and fumarate as well as both enantiomers of 2-hydroxyglutarate (D-2HG and L-2HG) (Tomlinson et al., 2002, Baysal et al., 2000, Niemann and Muller, 2000, Parsons et al., 2008, Yan et al., 2009, Green and Beer, 2010, Mardis et al., 2009). Notably, elevated oncometabolite levels are observed with inborn errors of metabolism, such as elevated fumarate due to fumarase deficiency. Both forms of 2HG may be elevated in the setting of acidurias related to loss of function mutations in either the D-2HG dehydrogenase (*D2HGDH*) or L-2HG dehydrogenase (*L2HGDH*) genes (Duran et al., 1980, Kranendijk et al., 2012, van der Knaap et al., 1999).

L-2HG has garnered recent interest as elevated levels are observed in several other settings besides inborn errors of metabolism. Multiple studies have demonstrated that L-2HG can be elevated in the setting of hypoxia (Oldham et al., 2015). Additionally, profound increases in L-2HG have been identified in *Drosophila* larval development (Li et al., 2017, Li et al., 2018). L-2HG can be created from α-ketoglutarate (α-KG) by off-target reactions of several enzymes, including lactate dehydrogenase and malate dehydrogenase 1 and 2 (MDH1/2) (Nadtochiy et al., 2016, Intlekofer et al., 2017, Rzem et al., 2007). L2HGDH activity serves to counter this off-target activity and therefore has been referred to as an enzyme of metabolic repair. In addition, L-2HG levels are also elevated in the most common histology (clear cell) of renal cell carcinoma (RCC) due to loss of expression of L2HGDH. Restoration of L2HGDH activity in several RCC models leads to reduced L-2HG levels. Moreover, reducing L-2HG impedes tumor growth *in vivo*, indicating that L-2HG promotes RCC growth. The *L2HGDH* gene is located on chromosome 14q, a region commonly deleted in RCC. As such, RCC tumors that exhibit 14q loss demonstrate reduced L2HGDH expression (Shelar et al., 2018, Shim and Sudarshan, 2015, Shim et al., 2014).

The cellular effects due to oncometabolite elevation have been the subject of interest since their initial identification. L-2HG, like other oncometabolites, is structurally similar to α-KG (also referred to as 2-oxoglutarate/2-OG). α-KG is a metabolite of the TCA cycle. Additionally, it serves as a co-factor for 2-oxoglutarate dependent dioxygenases. These enzymes mediate diverse processes including RNA, DNA, and histone demethylation. As such, prior studies have demonstrated increased DNA/RNA/histone methylation in oncometabolite-related tumors with corresponding gene

expression changes (Xu et al., 2011, Su et al., 2018, Shim et al., 2014). More recently, D-2HG has been shown to inhibit enzymes that utilize α-KG as a substrate, namely branched-chain aminotransferases (BCAT1/2) that metabolize branched-chain amino acids (McBrayer et al., 2018). These data would suggest that oncometabolites could act via effects on gene expression as well as direct effects on metabolism. Furthermore, several factors could impact the effects of an oncometabolite such as the type of oncometabolite, the α-KG level, the amount of target enzyme, and the affinity of the oncometabolite compared to α-KG. Thus, the effect could be tissue-specific and can fluctuate based on available nutrients.

Biallelic mutation of *L2HGDH* results in L-2HG aciduria, a neurometabolic inborn error of metabolism marked by neurologic deterioration and decreased life expectancy (Rzem et al., 2007). Notably, it is also associated with the development of brain tumors (Haliloglu et al., 2008). Recent studies have looked at the effects of whole-body *L2hgdh* knockout mouse models. Rzem *et al.* used a gene-trap cassette method which identified that L-2HG inhibits lysine α-ketoglutarate reductase/saccharopine dehydrogenase leading to depletion of saccharopine and glutamine in the brain (Rzem et al., 2015). Additionally, Ma *et al*. used a piggyback transposon gene insertion method to disrupt *L2hgdh*. These mice showed extensive brain abnormalities (Ma et al., 2017). These studies have provided insight into the role of L2HGDH in the brain. Although L2HGDH is known to prevent L-2HG elevation, the physiologic rationale for keeping L-2HG levels low remains largely unknown. Moreover, as the prior studies focused on brain findings, the teleologic role of this enzyme in other tissues where it is highly expressed remains unknown. Here, we report on the creation of a *L2hgdh* knockout model using CRISPR/Cas9 that recapitulates the brain abnormalities noted in prior knockout models. Additionally, we demonstrate a role for L2HGDH in mitochondrial metabolism in the kidney, a tissue with high basal L2HGDH expression. These data have implications for L-2HG's effects in both physiologic as well as pathologic states.

Methods

Lentivirus. L2HGDH (wild type) and L2HGDH mutant (A241G) cDNA are previously described (Shelar et al., 2018). To generate stable cell lines, lentiviral plasmids were transfected with packaging vectors into HEK293T cells using the calcium chloride method. Supernatants from transfected HEK293T cells were collected after 72h, filtered, and applied to cells. Viral transduced cells were selected in culture medium containing puromycin. All transduced cells represent polyclonal populations.

Adenovirus. PPARGC1A (encoding PGC-1α) and GFP control adenovirus were purchased from Vector Biolabs. Cells were analyzed 48-72 hours after transduction. A multiplicity of infection (MOI) of 100 was used for all experiments.

siRNA studies. Cells were seeded on 6 well plates for 48h. Cells were then transfected with 50 nM of a negative control siRNA or siRNA against PGC-1α using Lipofectamine® RNAiMAX regent (Invitrogen) for 48 h. Additional methods are described previously (Nam et al., 2020).

Generation of L2HGDH knockout mice. In order to create a loss of function alleles of the mouse *L2hgdh* gene (ENSMUSG00000020988), CRISPR targets were chosen in the coding region of exon 1 (ENSMUSE00000113742; Transcript ID ENSMUST00000021370.9) using the MIT CRISPR design tool (crispr.mit.edu). Two guide sequences with high scores that indicated a low number of off-target sites were chosen, C1: AGACACCGCCTACGTAGCGC(AGG) and C2: ACGCCGGTCCACTTGCGCGG (AGG). Guide RNA molecules were generated using the method described by Hwang and co-workers (Hwang et al., 2013). Cas9 mRNA was prepared by *in vitro* transcription using a linearized pCS2-nCas9n plasmid template (Jao et al., 2013).

Genotyping G0/founders and F1 animals to identify mutant alleles. Genotyping by PCR-heteroduplex mobility assay (HMA) was employed to identify indels in the G0/founder animals (Challa et al., 2016), using the primers: forward-5'-CCTTAGAGTCCGTTCAGGTTG-3'; reverse-5'-GGACACAGACAGGTTCAGTTG-3' that amplified a 271 bp fragment. The PCR amplicons were cloned and sequenced using the Sanger method to obtain the mutant allele information.

Pathology. Reproductive tissues were fixed in Bouin's solution before being processed. All other tissues were formalin-fixed before processing by the UAB Comparative Pathology Laboratory. Fixed tissue was placed onto slides and stained with H&E for analysis.

Mouse Tissue GC/MS. Mice were fasted for 12 hours before tissue isolation. Tissues were briefly washed in ice-cold in DPBS, followed by rapid freezing in liquid nitrogen. Metabolite extraction and derivatization were conducted using a modified version of previously described protocols (Chan et al., 2011; Gibson et al., 1993; Pasikanti et al., 2008). Briefly, samples were added to pre-tared 2 mL screw cap tubes containing 1.4 mm ceramic beads, massed, and 800 µl of -20ºC methanol with 2 µg/mL of both d4-succinic acid and disodium (R,S)-[2,3,3-2H3]-2-hydroxyglutarate ([2H3]-2HG) (C/D/N ISOTOPES INC., Canada) was added to the tube. Samples were homogenized in an Omni Beadruptor 24 for 30 second at 6.45 m/second, returned to a -20ºC benchtop enzyme cooler, and incubated at -20ºC for one hour. Samples were then centrifuged at ~20,000 x g in a refrigerated centrifuge for 5 minutes to pellet insoluble debris. Supernatant was removed, evenly split between two tubes, and dried in a vacuum centrifuge. One tube was derivatized using a previously described method to quantify D- and L-2HG levels. The second tube was derivatized using MOX and MSTFA to measure the relative abundance of organic acids, amino acids, and glycolytic intermediates. Derivatized samples were injected into an Agilent 7890B/7250 GC-QTOF instrument (1:10 split ratio) equipped with a Phenomex ZB5-5 MSi column using a Gerstel MPS autosampler using previously described methods (Li and Tennessen, 2018; Li and Tennessen, 2019). Data were analyzed using MassHunter Qualitative Analysis and MassHunter Quantitative Analysis. Power analysis based on preliminary data was calculated with a mu1: 1, mu2:1.5, sigma of 0.25 alpha: 0.05, and power: 0.8 demonstrated a minimal need of 4 mice. We used n=5 mice in this analysis. Both groups included both male and female mice.

Cell Culture. Renal cell lines were acquired from ATCC except for RXF-393 (NCI). Cells acquired from ATCC and NCI were characterized via short tandem repeat (STR) profiling. As cells were passaged for less than three months after resuscitation and were periodically screened for *Mycoplasma* using a PCR-based assay, no further authentication was performed. HEK293T and Caki-1 were maintained with DMEM containing 10% FBS and penicillin/streptomycin. RXF-393, 769P, and 786O cells were

maintained in RPMI containing 10% FBS and penicillin/streptomycin. Phenotype/genotype information for cell lines used including L2HGDH expression, *VHL* status, and copy number status is provided in fig. S1.

Bioinformatics/TCGA analysis. Co-expression analysis of TCGA data on clear cell renal cancer (KIRK) was performed using the "GRACE" analysis tool (https://grace.biohpc.swmed.edu/) (Cai et al., 2017) as well as the cBIO analysis portal (www.cbioportal.org) (Gao et al., 2013, Cerami et al., 2012). Kyoto encyclopedia of Genes and Genomes (KEGG) (https://www.genome.jp/kegg/) (Kanehisa and Goto, 2000, Kanehisa et al., 2019, Kanehisa, 2019) was used for pathway mapping. Pathway analysis was performed by Enrichr (Chen et al., 2013, Kuleshov et al., 2016) (https://amp.pharm.mssm.edu/Enrichr/). Enrichment analysis performed by Webgestalt (http://www.webgestalt.org/) (Liao et al., 2019, Wang et al., 2017, Wang et al., 2013, Zhang et al., 2005).

α-KGDH Assay. The enzymatic assay was obtained from BioVision. For cell-independent experiments, α-KGDH enzyme and necessary coenzymes were incubated with increasing concentrations of L-2HG. L-2HG was synthesized as previously described (Shim et al., 2014). OD readings at 450nm were taken every 5 minutes over 70 minutes.

Tumor copy number analysis. Clear cell RCCs and normal tissues were acquired from the Cooperative Human Tissue Network. DNA was isolated from tissues using the Qiagen DNeasy Blood and Tissue kit. Gene copy number was determined using commercially-available TaqMan Copy Number assays with FAM dye-labeled probes: Hs02530250_cn (HIF1A), and Hs07069935_cn (L2HGDH (ThermoFisher). The TERT TaqMan copy number reference with a VIC dye-labeled probe (4403316) was used as the two copy reference (ThermoFisher). The PCR reactions were performed in triplicate in a twenty microliter reaction containing 80 nanograms of DNA, 1X TaqMan Universal PCR Master Mix (ThermoFisher), 1X gene-specific Copy Number Assay and 1X Copy Number Reference Assay. The reactions were cycled at 95^{o}C for 10 minutes, followed by 40 cycles of 95^{o}C for 15 seconds and 60^{o}C for 1 minute in a BioRad CFX96 Touch Real-Time PCR system. Cq (Ct) values were determined using the CFX Manager software (BioRad). Gene copy numbers for the test samples were determined using the 2^-ΔΔCq method with a two copy calibrator.

RNA and protein analysis. Total RNA from cultured cells was extracted using Trizol reagent (Invitrogen). cDNA was synthesized using the High-Capacity cDNA Reverse Transcription Kit (ThermoFisher). Real-time qPCR was performed using the following TaqMan gene expression assays (Thermo): L2HGDH (Hs00227575), PPARGC1A (Hs00173304_m1), MDH1 (Hs00936497_g1), MDH2 (Hs00938918_m1), ACO2 (Hs00426616_g1) and OGDH (Hs01081865_m1). HPRT1 (Hs02800695_m1) and RPLPO (hs99999902_m1) probes were used as an internal control, and the ΔΔCt method was used to calculate relative mRNA levels. For immunoblotting, α-L2HGDH (GeneTex, #GTX32695 1:2000 and Novus, NBP2-85197 1:1000), α-PGC1 alpha (Abcam, #AB54481 1:1000) α-MDH2 (Abcam, #ab96193 1:3000), MDH1 (Novus, #NBP1-895151 1:3000) and β-actin (Abcam, #ab20272 1:3000) were used as per manufacturers' instructions.

2HG enantiomer analysis (i.e., D- and L-2HG quantification): Samples were analyzed as previously described (Rakheja et al., 2011). Enantiomer analysis was performed following derivatization with DATAN (diacetyl-L-tartaric acid followed by liquid chromatography-tandem mass spectrometry (LC-MS/MS) analysis and normalized to protein levels.

Total 2HG measurements. Total 2HG (D-2HG+L-2HG) measurement of samples from renal tissues was performed as previously described (Shim et al., 2014). Briefly, tissues were washed in PBS, followed by extractions with 10% cold trichloroacetic acid (TCA). Following centrifugation and removal of the precipitate, TCA in the supernatant was removed by vortexing with four volumes of 1,1,2-trichlorotrifluoroethane (FREON)-trioctylamine (Sigma) mixture. The aqueous layer was collected and analyzed by ion chromatography coupled with negative electrospray mass spectrometry (RFIC-MS) (Dionex).

LC/MS isotope labelling analysis. Cells were plated with RPMI with 10% dialyzed FBS, and Pen/Strep. After 24hrs, [U-^{13}C]-glucose was added to the media for 24 hrs. Cells were then washed with ice cold 0.9% NaCl in molecular grade water. Cells were lysed in 80% LCMS methanol and scraped into 1.5cc conical vials. Cells were then placed in at -80^{o}C and processed further processed on dry ice. Cells were spun at full speed for 20 minutes at 4^{0}C. Supernatant was split between two samples and dry vacuumed at room temperature until no liquid remained. The dry pellets were reconstituted into 30 ml sample

solvent (water:methanol:acetonitrile, 2:1:1, v/v) and 3 ml was further analyzed by liquid chromatography-mass spectrometry (LC-MS). A detailed LC method was described previously (Liu et al., 2015)((Liu et al., 2014)) except that mobile phase A was replaced with water containing 5mM ammonium acetate (pH 6.8). The QE-MS is equipped with a HESI probe with related parameters set as below: heater temperature, 120 °C; sheath gas, 30; auxiliary gas, 10; sweep gas, 3; spray voltage, 3.0 kV for the positive mode and 2.5 kV for the negative mode; capillary temperature, 320 °C; S-lens, 55; scan range (m/z): 70 to 900 for pos mode (1.31 to 12.5 min) and neg mode (1.31 to 6.6 min) and 100 to 1000 for neg mode (6.61 to 12.5 min); resolution: 70000; automated gain control (AGC), 3 × 106 ions. Customized mass calibration was performed before data acquisition. LC-MS peak extraction and integration were performed using commercially available software Sieve 2.2 (ThermoFisher). The peak area was used to represent the relative abundance of each metabolite in different samples. The missing values were handled as described in a previous study (Liu et al., 2014).

Statistical Analysis. Statistical analyses were carried out using GraphPad Prism6 software. Comparisons between groups for statistical significance were performed with a two-tailed t-tests with a $p<0.05$ for significance unless otherwise specified.

Study Approval. All mouse experiments were performed following the Guide for the Care and Use of Laboratory Animals published by the National Institutes of Health and experimental protocols were approved and conducted according to the University of Alabama at Birmingham IACUC.

Results

Generation of L2HGDH knockout with CRISPR/Cas9.

CRISPR/Cas9 genome editing was used to generate a deletion in *L2hgdh*, causing a mutant allele with an 11 base pair deletion. This deletion results in a frameshift very early in exon 1, encoding the initial 22 amino acids followed by 24 mutant amino acids and a stop codon (Fig. 1A). We inferred this allele to result in a complete loss-of-function of the *L2hgdh* gene. This allele was successfully transmitted through the germline, enabling us to establish a knockout line. Protein analysis of both kidney and liver tissues demonstrates loss of *L2hgdh* expression relative to WT animals. (Fig. 1B, C). We next analyzed D- and L-2HG levels via GC/MS in liver, kidney, and gastrocnemius (striated) muscle. As heterozygous mice demonstrated comparable L-2HG levels in all three tissues as compared to WT (+/+) mice (Fig. S2), littermate control mice included both +/+ and +/- genotypes. Consistent with loss of *L2hgdh* activity, L-2HG levels were elevated in all tissues from knockout animals as compared with control animals. Moreover, kidney demonstrated a much higher abundance of L-2HG relative to other tissues (Fig. 1D). This differs from a prior report which found similar levels of L-2HG amongst these tissues in knockout mice (Ma et al., 2017). Additionally, all three tissues from knockout animals demonstrated a modest increase in D-2HG with kidney tissue demonstrating the highest increase (Fig. 1E).

Histologic analysis of the brain and kidney.

Histologic analysis of the brain was performed in 24-week-old mice. When compared to the *L2hgdh*$^{+/+}$ mice, the brains of *L2hgdh*$^{-/-}$ mice consistently showed spongiotic appearance and perineuronal vacuoles, predominantly seen in the deep layers of the cerebral cortex consistent with prior knockout models reported (Fig. 2A). The examination of the kidney did not demonstrate any significant differences in gross examination (Fig. 2B). Remarkably, no significant histologic difference was noted when comparing the kidneys from the *L2hgdh*$^{+/+}$ and *L2hgdh*$^{-/-}$ mice (Fig. 2C).

Decreased fertility in L2hgdh$^{-/-}$ *male mice*

We observed that *L2hgdh*$^{-/-}$ male mice had significantly reduced fertility when bred with *L2hgdh*$^{+/-}$ females (Fig. 3A). Out of three attempts at breeding, only one produced pups. Moreover, this litter had only two pups. This is in stark contrast to the pairing of *L2hgdh*$^{+/-}$ mice that produced an average of 7 pups per litter. Histologic analysis of testes and accessory sex glands did not demonstrate any differences between WT and KO males (Fig. 3B and data not shown).

Reduced succinate in tissues with high L-2HG

Prior metabolomics studies in *L2hgdh* KO mice focused on the brain (Rzem et al., 2015). However, tissues including kidney, liver, and skeletal muscle also express high levels of this enzyme with the kidney being the highest-expressing tissue in humans (Fig. S2). We therefore performed metabolic profiling in these tissues (in addition to serum) that included small molecules from pathways including glycolysis, the TCA cycle, as well as amino acid metabolism (data provided in Table S1). Notably, TCA cycle metabolites were not measured in previous *L2hgdh* KO mice models. To minimize the potential effects of the diet, we fasted the mice for 12 hours before tissue isolation. (n=5/group including both male and female mice). Analysis of tissues from knockout mice demonstrated significantly decreased succinate in both kidney (p= 0.0106) and muscle (p=0.001). Additionally, this decrease in succinate was trending toward significance in serum as well (p=0.090). There were also several amino acids (threonine, tyrosine, and lysine) trending toward decreased levels in KO kidneys whose p values were approaching significance (Fig.1A).

L2HGDH restoration promotes TCA cycle flux

Succinate is a known metabolite of the TCA cycle and is generated by the enzyme succinyl-CoA ligase. As decreased succinate was observed in multiple knockout tissues, we considered the possibility of whether elevations of L-2HG could perhaps impact the TCA cycle. From previous studies, we found that 769-P RCC cells had reduced L2HGDH expression with concomitant L-2HG elevation (Shelar et al., 2018). We have previously demonstrated that the restoration of L2HGDH expression significantly lowers L-2HG levels. We therefore assessed the effects of L2HGDH on the TCA cycle. 769-P cells +/- L2HGDH were then cultured with fully labeled glucose [U-^{13}C] followed by LC-MS analysis). For the analysis, we measured total label incorporation for metabolites of interest. We did not observe a significant difference in label incorporation into citrate/isocitrate or α-KG (Fig. 5). However, we observed that L2HGDH restoration led to increased label incorporation into the TCA cycle metabolites succinate (p=0.011) and malate (p=0.019) (Fig. 5). We also observed that L2HGDH led to increased label incorporation into amino acids including aspartate (p=0.017) and alanine (p=0.007). Notably, aspartate is known to be generated by transamination of the TCA cycle intermediate oxaloacetate. No significant difference in glucose (both labeled and unlabeled) was observed as a function of L2HGDH (Table S2).

Impact of L-2HG on the TCA cycle

As noted, α-KG-dependent dioxygenases are known to catalyze the demethylation of DNA, RNA, as well as histones. Therefore, oncometabolites may impact gene expression via effects on transcription and/or protein translation. Prior analyses demonstrate reduced expression of TCA cycle enzyme expression in RCC specimens (Cancer Genome Atlas Research, 2013, Wettersten, 2020). We therefore considered if L-2HG suppressed the expression of TCA cycle enzymes, thereby leading to reduced TCA cycle flux. We restored L2HGDH (both WT and A241G mutant) in 786O and 769-P RCC cells. As expected, WT L2HGDH lowers L-2HG, whereas the mutant does not affect L-2HG levels (S2A-B). In both cell lines, modulation of L-2HG levels had no impact on TCA cycle enzyme mRNA or protein expression (S2C-E).

We, therefore, considered alternative mechanisms by which L-2HG could impact the TCA cycle. Recent studies demonstrate that D-2HG can inhibit enzymes that utilize α-KG as a substrate. Within the TCA cycle, α-KG dehydrogenase (α-KGDH) converts α-KG to succinyl-CoA, which is subsequently converted to succinate. In turn, succinate is converted to other TCA cycle intermediates (e.g. malate) as well as metabolites derived from TCA cycle intermediates (e.g. aspartate). Based on our findings related to the TCA cycle, we hypothesized that L-2HG could directly inhibit the enzymatic activity of α-KGDH (Fig. 6A). Using an *in vitro* biochemical assay, we observed that L-2HG led to a dose-dependent inhibition of α-KGDH enzymatic activity (Fig. 6B).

These biochemical data led us to surmise that the teleological role for L2HGDH in the kidney is to keep L-2HG levels low such that TCA cycle flux is maintained. To further support this role for L2HGDH, we examined co-regulated genes within the TCGA data set on clear cell RCC (KIRK) using the Genomic Regression Analysis of Coordinated Expression (GRACE) tool (Cai et al., 2017) (Table S3). This algorithm performs co-expression analyses while accounting for the potential effects of copy number alterations, which commonly occur in cancers. This is particularly relevant as copy number loss of *L2HGDH* is found in 42.5% of clear cell RCC patients based on TCGA analysis (data not shown). Using a Spearman Rho rank threshold of 0.3 (at least moderate association), we performed a pathway analysis of positivity associated genes with the Enrichr tool (https://amp.pharm.mssm.edu/Enrichr/). This analysis demonstrated that *L2HGDH* is coordinately expressed with genes involved in pathways including branched-chain amino acid (BCAA) degradation, peroxisomes, fatty acid metabolism as well as the TCA cycle

(Fig. 6C). TCA cycle genes that positively correlate with *L2HGDH* are shown in Fig. 6D. Utilizing the Spearman rank rho for rank order of genes from the GRACE analysis, we performed pathway analysis utilizing all genes with the Webgestalt tool. Fig. 6E displays the TCA cycle enrichment plot from the analysis. Both FDR and p-value were <.001. These bioinformatics analyses provide further evidence of L2HGDH's role in promoting TCA cycle metabolism, which corresponds with our biochemical studies.

An alternative mechanism for reduced L2HGDH and elevated L-2HG.

L-2HG build-up in RCC is due to loss of L2HGDH expression. Our lab has previously reported that 14q loss, the chromosomal location for the *L2HGDH* gene, is significantly associated with decreased *L2HGDH* mRNA. Notably, heterozygous loss of *L2hgdh* in mice (*L2hgdh*$^{+/-}$) resulted in reduced L2HGDH protein (Fig. 7A) but was not sufficient to significantly increase 2HG levels in the kidney (Fig. 7B). Only homozygous loss of *L2hgdh* led to increased 2HG in the kidney. These data suggest that while gene copy loss can reduce L2HGDH expression, this mechanism alone does not result in raised L-2HG and that alternative mechanisms exist that reduce L2HGDH in RCC to the point that L-2HG becomes elevated.

As further supportive evidence, we analyzed L2HGDH mRNA expression and gene copy number in normal kidney and RCC specimens. RCC specimens were separated into high and low L-2HG tumors based on whether levels were within two standard deviations of normal kidney median. A log-log plot of linear regression analysis identified a negative correlation with a R^2 of 0.1410 (Fig. 7C). Next, we analyzed high L-2HG tumors for *L2HGDH* copy loss. While 8 of 13 high L-2HG tumors demonstrated *L2HGDH* copy loss, we noted five tumors with raised L-2HG without evidence of copy loss (Fig.7D). As a control for our copy number analysis, we examined *HIF1A*, which is also located on 14q. Of the eight high L-2HG tumors which demonstrated *L2HGDH* copy loss (monoallelic loss), six tumors also demonstrated *HIF1A* copy loss (Fig. 7E). Correspondingly, of the five high L-2HG tumors without *L2HGDH* copy loss, four tumors did not demonstrate *HIF1A* loss. Collectively, these data further support our findings that alternative mechanisms can promote loss of L2HGDH expression with ensuing elevated L-2HG in RCC.

Based on the combined analysis of our knockout model and biospecimens, we sought to identify alternative mechanisms for reduced L2HGDH/elevated L-2HG in RCC. Utilizing our information from pathway analysis of genes coregulated with *L2HGDH*, we attempted to identify potential transcription factors which 1) are known to regulate mitochondrial metabolic pathways and 2) are reduced in RCC. One such transcription factor identified was the gene *PPARGC1A,* which encodes peroxisome proliferator-activated receptor gamma coactivator 1-alpha (PGC-1α). Our laboratory recently reported on reduced PGC-1α in RCC tissues and reported on multiple RCC lines with reduced expression (Nam et al., 2020). Analysis of TCGA data on clear cell RCC demonstrates that *PPARGC1A* and *L2HGDH* mRNA are positively correlated (Fig. 8A). Restoration of PGC-1α expression via adenovirus increased the mRNA expression of *L2HGDH* in multiple RCC lines examined (Fig. 8B). Furthermore, stable expression of PGC-1α via lentiviral transduction in RXF-393 cells increased L2HGDH protein and significantly reduced L-2HG levels (Fig. 8C-D). Additionally, knockdown of *PPARGC1A* utilizing siRNA decreased L2HGDH protein in both HK2 renal epithelial cells and HEK293T embryonic kidney cells (Figs. 8E and S5). *PPARGC1A* knockdown was confirmed by qPCR (Fig. 8F). Collectively these data demonstrate a role for PGC-1α in regulating L2HGDH expression and L-2HG levels.

Discussion

L-2HG can have widespread effects on a cell. L-2HG has been shown to competitively inhibit enzymes that utilize α-KG as a co-factor with effects on DNA and histone methylation. Finding the models to reflect the most impactful effects of L-2HG accurately is essential to better understand its role in cancer, hypoxia, and development. There is an abundance of different techniques that can be used for *in vivo* gene-edited mouse models. Recent studies have shifted to CRISPR/Cas9 for both its ease to generate models and its specificity (Weber and Rad, 2019). We thus compared our new model to previous models and found similar characteristics. All models showed increased L-2HG in all tissues tested and abnormal pathology in brain tissue (Rzem et al., 2015, Ma et al., 2017). Unlike previous models, our *L2hgdh* KO mouse model demonstrated more pronounced L-2HG elevation in the kidney compared to the liver and muscle. Moreover, knockout males showed significantly reduced fertility (Fig. 3). Testes are also known to express L2HGDH. Notably, rodent testes express a variant of LDH-C, which can produce high levels of L-2HG (Teng et al., 2016).

We used this model to examine the biochemical implications of raised L-2HG in the kidney, the tissue with the highest expression of L2HGDH in humans (Fig. S2). We used a metabolomic approach to study L-2HG's effect. Our GC/MS analysis of the kidney and muscle tissues demonstrated a significant decrease in succinate levels as compared to control mice (p=.01 and .001, respectively), leading us to hypothesize a link between L-2HG and the TCA cycle. Interestingly, KO liver did not show a significant difference in succinate levels. One possible explanation is that the degree of L-2HG elevation in KO liver was less than that observed in kidney and muscle (Fig. 1D). Alternatively, these data may indicate that L-2HG's effects are tissue-dependent.

The link between L-2HG and the TCA cycle is particularly intriguing as RCC tumors are known to demonstrate reduced expression of TCA cycle enzymes (Cancer Genome Atlas Research, 2013). Correspondingly, isotope labeling studies by Courtney *et al.* with [U-^{13}C] glucose in patients provided a reference for interpretation of our studies. Courtney *et al.* demonstrates reduced TCA cycle labeling in RCC relative to normal kidney (Courtney et al., 2018). Reintroduction of L2HGDH back into RCC cells led to increased ^{13}C labeling of TCA cycle metabolites, including succinate and malate as well as metabolites derived from the TCA cycle such as aspartate. Interestingly, there were no significant differences in the labeling of TCA metabolites earlier in the cycle (citrate/isocitrate and α-KG). Similarly, Courtney *et al.* found reduced labeling in TCA cycle metabolites in succinate, fumarate, and malate but no metabolites earlier in the cycle such as citrate. These data led us to focus on α-KGDH. As further evidence for a link between L-2HG and α-KGDH, bacterial species of *Marinomonas* often demonstrate the clustering of αKGDH subunit genes and *ygaF*, the gene encoding the bacterial equivalent of L2HGDH (Seaver et al., 2012). These data would reinforce the role of L2HGDH as an enzyme of metabolite repair by keeping L-2HG levels "in check" such that α-KGDH activity is maintained. One caveat to our studies is that alternative carbon sources may contribute to TCA cycle anaplerosis. This is partiucarly relevant as glucose entry into the TCA cycle is impaired in RCC due to HIF-mediated inhibition of pyruvate dehydrogenase(Papandreou et al., 2006, Kim et al., 2006). For example, glutamine can be metabolized to α-KG. Hence, raised L-2HG could impact the anaplerotic role of these alternative carbon sources.

Our data demonstrate that L-2HG promotes TCA cycle dysfunction and provides new insight into the mechanisms that lead to a classic Warburg phenotype in RCC. Despite these data, the true biologic significance remains poorly characterized. At the

same time, it may provide new opportunities for intervention. The TCA cycle represents a major bioenergetic hub with cataplerotic activities that are known to have biosynthetic functions. Hence, raised L-2HG may create potential liabilities that could be used for treating tumors. Alternatively, potential deficiencies resulting from this liability could be supplemented for patients with 2HG acidurias.

Our study of this model has provided new insight into the regulation of L2HGDH based on our finding that biallelic loss of *L2hgdh* was required to raise renal L-2HG levels. These data indicate that single copy loss of *L2HGDH* alone is not sufficient enough to lower L2HGDH expression to the point that L-2HG levels are increased in kidney tumors. As further evidence, we identified several renal tumors with low *L2HGDH* expression/elevated L-2HG without *L2HGDH* copy loss. These data allude to the importance of L-2HG in RCC in that reduced *L2HGDH* expression is not merely a bystander effect associated with copy loss, but instead that there is a concerted effort to silence this gene in RCC.

Our studies demonstrate new insight into PGC-1α's role in mitochondrial metabolism. PGC-1α has been shown promote oxidative metabolism via transcriptional regulation of genes encoding oxidative phosphorylation subunits and TCA cycle enzymes (LaGory et al., 2015, Calvo et al., 2008, Koves et al., 2005, Bhalla et al., 2011). Our data demosntrate that PGC-1α also promotes TCA cycle metabolism via *L2HGDH* transcription which lowers L-2HG levels. One caveat of these experiments is that all cell lines examined have a heterozygous loss of *L2HGDH* (Fig. S1). As a result, the effects of PGC-1α on *L2HGDH* transcription may be dampened. While L-2HG does not have effects on the expression of TCA cycle enzymes in RCC, it can affect TCA cycle metabolism. As a result of low L-2HG levels, α-KGDH activity is maintained thereby promoting TCA cycle flux. These data would, therefore, indicate that the teleological role for L2HGDH, at least in the kidney, is to promote mitochondrial metabolism, which is in line with our biochemical findings. Our findings are consistent with previous work demonstrating that high D-2HG levels can lower α-KGDH activity in cardiac muscle tissue. However, the direct inhibitory role of D-2HG on α-KGDH enzymatic activity was not examined (Karlstaedt et al., 2016). These data are in line with prior studies that have demosntrated that both enantiomers of 2HG can inhibit enzymes that utilize α-KG as a cofactor or susbtrate. Our studies focused on L-2HG because D-2HG is not significantly elevated in RCC. Further studies on the effects D-2HG on TCA cycle metabolism in *IDH* mutant tumors would be of interest.

In summary, this report highlights the creation and analysis of a novel *L2hgdh* KO mouse model in concert with human RCC tissues to study the metabolite L-2HG. We demonstrate a role for L2HGDH in promoting mitochondrial metabolism in the kidney. These data provide new insights into the pathophysiologic implications of raised L-2HG and may provide new avenues for therapeutic intervention.

Author Contributions

GB, HN, ES, RK, AK, SK, YH, JL and DR acquired data. JMT, JWL, TG, SW, JG, and TJ analyzed data. AC generated reagents. GB and SS contributed to the conception, design as well as writing.

Acknowledgements

The research reported in this article was supported by R01CA200653 and I01BX002930 (to S.S.), F30CA232397 (to G.B) and in part by the UAB O'Neal Comprehensive Cancer Center (P30CA013148) and T32 GM008361. Tumor genotyping was supported in part by the UT Health San Antonio Mays Cancer Center Genomics Shared Resource Facility (P30 CA054174). J.M.T. is supported by a MIRA award from NIGMS (R35GM119557). We would also like to acknowledge the assistance of the UAB Transgenic and Genetically Engineered Models Core and Comparative Pathology Laboratory.

References

BAYSAL, B. E., FERRELL, R. E., WILLETT-BROZICK, J. E., LAWRENCE, E. C., MYSSIOREK, D., BOSCH, A., VAN DER MEY, A., TASCHNER, P. E., RUBINSTEIN, W. S., MYERS, E. N., RICHARD, C. W., 3RD, CORNELISSE, C. J., DEVILEE, P. & DEVLIN, B. 2000. Mutations in SDHD, a mitochondrial complex II gene, in hereditary paraganglioma. *Science,* 287**,** 848-51.

BHALLA, K., HWANG, B. J., DEWI, R. E., OU, L., TWADDEL, W., FANG, H. B., VAFAI, S. B., VAZQUEZ, F., PUIGSERVER, P., BOROS, L. & GIRNUN, G. D. 2011. PGC1alpha promotes tumor growth by inducing gene expression programs supporting lipogenesis. *Cancer Res,* 71**,** 6888-98.

CAI, L., LI, Q., DU, Y., YUN, J., XIE, Y., DEBERARDINIS, R. J. & XIAO, G. 2017. Genomic regression analysis of coordinated expression. *Nat Commun,* 8**,** 2187.

CALVO, J. A., DANIELS, T. G., WANG, X., PAUL, A., LIN, J., SPIEGELMAN, B. M., STEVENSON, S. C. & RANGWALA, S. M. 2008. Muscle-specific expression of PPARgamma coactivator-1alpha improves exercise performance and increases peak oxygen uptake. *J Appl Physiol (1985),* 104**,** 1304-12.

CANCER GENOME ATLAS RESEARCH, N. 2013. Comprehensive molecular characterization of clear cell renal cell carcinoma. *Nature,* 499**,** 43-9.

CERAMI, E., GAO, J., DOGRUSOZ, U., GROSS, B. E., SUMER, S. O., AKSOY, B. A., JACOBSEN, A., BYRNE, C. J., HEUER, M. L., LARSSON, E., ANTIPIN, Y., REVA, B., GOLDBERG, A. P., SANDER, C. & SCHULTZ, N. 2012. The cBio cancer genomics portal: an open platform for exploring multidimensional cancer genomics data. *Cancer Discov,* 2**,** 401-4.

CHEN, E. Y., TAN, C. M., KOU, Y., DUAN, Q., WANG, Z., MEIRELLES, G. V., CLARK, N. R. & MA'AYAN, A. 2013. Enrichr: interactive and collaborative HTML5 gene list enrichment analysis tool. *BMC Bioinformatics,* 14**,** 128.

COURTNEY, K. D., BEZWADA, D., MASHIMO, T., PICHUMANI, K., VEMIREDDY, V., FUNK, A. M., WIMBERLY, J., MCNEIL, S. S., KAPUR, P., LOTAN, Y., MARGULIS, V., CADEDDU, J. A., PEDROSA, I., DEBERARDINIS, R. J., MALLOY, C. R., BACHOO, R. M. & MAHER, E. A. 2018. Isotope Tracing of Human Clear Cell Renal Cell Carcinomas Demonstrates Suppressed Glucose Oxidation In Vivo. *Cell Metab,* 28**,** 793-800 e2.

DURAN, M., KAMERLING, J. P., BAKKER, H. D., VAN GENNIP, A. H. & WADMAN, S. K. 1980. L-2-Hydroxyglutaric aciduria: an inborn error of metabolism? *J Inherit Metab Dis,* 3**,** 109-12.

GAO, J., AKSOY, B. A., DOGRUSOZ, U., DRESDNER, G., GROSS, B., SUMER, S. O., SUN, Y., JACOBSEN, A., SINHA, R., LARSSON, E., CERAMI, E., SANDER, C. & SCHULTZ, N. 2013. Integrative analysis of complex cancer genomics and clinical profiles using the cBioPortal. *Sci Signal,* 6**,** pl1.

GREEN, A. & BEER, P. 2010. Somatic mutations of IDH1 and IDH2 in the leukemic transformation of myeloproliferative neoplasms. *N Engl J Med,* 362**,** 369-70.

HALILOGLU, G., JOBARD, F., OGUZ, K. K., ANLAR, B., AKALAN, N., COSKUN, T., SASS, J. O., FISCHER, J. & TOPCU, M. 2008. L-2-hydroxyglutaric aciduria and brain tumors in children with mutations in the L2HGDH gene: neuroimaging findings. *Neuropediatrics,* 39**,** 119-22.

HWANG, W. Y., FU, Y., REYON, D., MAEDER, M. L., TSAI, S. Q., SANDER, J. D., PETERSON, R. T., YEH, J. R. & JOUNG, J. K. 2013. Efficient genome editing in zebrafish using a CRISPR-Cas system. *Nat Biotechnol,* 31**,** 227-9.

INTLEKOFER, A. M., WANG, B., LIU, H., SHAH, H., CARMONA-FONTAINE, C., RUSTENBURG, A. S., SALAH, S., GUNNER, M. R., CHODERA, J. D., CROSS, J. R. & THOMPSON, C. B. 2017. L-2-Hydroxyglutarate production arises from noncanonical enzyme function at acidic pH. *Nat Chem Biol,* 13**,** 494-500.

JAO, L. E., WENTE, S. R. & CHEN, W. 2013. Efficient multiplex biallelic zebrafish genome editing using a CRISPR nuclease system. *Proc Natl Acad Sci U S A,* 110**,** 13904-9.

KANEHISA, M. 2019. Toward understanding the origin and evolution of cellular organisms. *Protein Sci,* 28**,** 1947-1951.

KANEHISA, M. & GOTO, S. 2000. KEGG: kyoto encyclopedia of genes and genomes. *Nucleic Acids Res,* 28**,** 27-30.

KANEHISA, M., SATO, Y., FURUMICHI, M., MORISHIMA, K. & TANABE, M. 2019. New approach for understanding genome variations in KEGG. *Nucleic Acids Res,* 47**,** D590-D595.

KARLSTAEDT, A., ZHANG, X., VITRAC, H., HARMANCEY, R., VASQUEZ, H., WANG, J. H., GOODELL, M. A. & TAEGTMEYER, H. 2016. Oncometabolite d-2-hydroxyglutarate impairs alpha-ketoglutarate dehydrogenase and contractile function in rodent heart. *Proc Natl Acad Sci U S A,* 113**,** 10436-41.

KIM, J. W., TCHERNYSHYOV, I., SEMENZA, G. L. & DANG, C. V. 2006. HIF-1-mediated expression of pyruvate dehydrogenase kinase: a metabolic switch required for cellular adaptation to hypoxia. *Cell Metab,* 3**,** 177-85.

KOVES, T. R., NOLAND, R. C., BATES, A. L., HENES, S. T., MUOIO, D. M. & CORTRIGHT, R. N. 2005. Subsarcolemmal and intermyofibrillar mitochondria play distinct roles in regulating skeletal muscle fatty acid metabolism. *Am J Physiol Cell Physiol,* 288**,** C1074-82.

KRANENDIJK, M., STRUYS, E. A., SALOMONS, G. S., VAN DER KNAAP, M. S. & JAKOBS, C. 2012. Progress in understanding 2-hydroxyglutaric acidurias. *J Inherit Metab Dis,* 35**,** 571-87.

KULESHOV, M. V., JONES, M. R., ROUILLARD, A. D., FERNANDEZ, N. F., DUAN, Q., WANG, Z., KOPLEV, S., JENKINS, S. L., JAGODNIK, K. M., LACHMANN, A., MCDERMOTT, M. G., MONTEIRO, C. D., GUNDERSEN, G. W. & MA'AYAN, A. 2016. Enrichr: a comprehensive gene set enrichment analysis web server 2016 update. *Nucleic Acids Res,* 44**,** W90-7.

LAGORY, E. L., WU, C., TANIGUCHI, C. M., DING, C. C., CHI, J. T., VON EYBEN, R., SCOTT, D. A., RICHARDSON, A. D. & GIACCIA, A. J. 2015. Suppression of PGC-1alpha Is Critical for Reprogramming Oxidative Metabolism in Renal Cell Carcinoma. *Cell Rep,* 12**,** 116-127.

LI, H., CHAWLA, G., HURLBURT, A. J., STERRETT, M. C., ZASLAVER, O., COX, J., KARTY, J. A., ROSEBROCK, A. P., CAUDY, A. A. & TENNESSEN, J. M. 2017. Drosophila larvae synthesize the putative oncometabolite L-2-hydroxyglutarate during normal developmental growth. *Proc Natl Acad Sci U S A,* 114**,** 1353-1358.

LI, H., HURLBURT, A. J. & TENNESSEN, J. M. 2018. A Drosophila model of combined D-2- and L-2-hydroxyglutaric aciduria reveals a mechanism linking mitochondrial citrate export with oncometabolite accumulation. *Dis Model Mech,* 11.

LIAO, Y., WANG, J., JAEHNIG, E. J., SHI, Z. & ZHANG, B. 2019. WebGestalt 2019: gene set analysis toolkit with revamped UIs and APIs. *Nucleic Acids Res,* 47**,** W199-W205.

LIU, X., SADHUKHAN, S., SUN, S., WAGNER, G. R., HIRSCHEY, M. D., QI, L., LIN, H. & LOCASALE, J. W. 2015. High-Resolution Metabolomics with Acyl-CoA Profiling Reveals Widespread Remodeling in Response to Diet. *Mol Cell Proteomics,* 14**,** 1489-500.

LIU, X., SER, Z. & LOCASALE, J. W. 2014. Development and quantitative evaluation of a high-resolution metabolomics technology. *Anal Chem,* 86**,** 2175-84.

MA, S., SUN, R., JIANG, B., GAO, J., DENG, W., LIU, P., HE, R., CUI, J., JI, M., YI, W., YANG, P., WU, X., XIONG, Y., QIU, Z., YE, D. & GUAN, K. L. 2017. L2hgdh Deficiency Accumulates l-2-Hydroxyglutarate with Progressive Leukoencephalopathy and Neurodegeneration. *Mol Cell Biol,* 37.

MARDIS, E. R., DING, L., DOOLING, D. J., LARSON, D. E., MCLELLAN, M. D., CHEN, K., KOBOLDT, D. C., FULTON, R. S., DELEHAUNTY, K. D., MCGRATH, S. D., FULTON, L. A., LOCKE, D. P., MAGRINI, V. J., ABBOTT, R. M., VICKERY, T. L., REED, J. S., ROBINSON, J. S., WYLIE, T., SMITH, S. M., CARMICHAEL, L., ELDRED, J. M., HARRIS, C. C., WALKER, J., PECK, J. B., DU, F., DUKES, A. F., SANDERSON, G. E., BRUMMETT, A. M., CLARK, E., MCMICHAEL, J. F., MEYER, R. J., SCHINDLER, J. K., POHL, C. S., WALLIS, J. W., SHI, X., LIN, L., SCHMIDT, H., TANG, Y., HAIPEK, C., WIECHERT, M. E., IVY, J. V., KALICKI,

J., ELLIOTT, G., RIES, R. E., PAYTON, J. E., WESTERVELT, P., TOMASSON, M. H., WATSON, M. A., BATY, J., HEATH, S., SHANNON, W. D., NAGARAJAN, R., LINK, D. C., WALTER, M. J., GRAUBERT, T. A., DIPERSIO, J. F., WILSON, R. K. & LEY, T. J. 2009. Recurring mutations found by sequencing an acute myeloid leukemia genome. *N Engl J Med,* 361**,** 1058-66.

MCBRAYER, S. K., MAYERS, J. R., DINATALE, G. J., SHI, D. D., KHANAL, J., CHAKRABORTY, A. A., SAROSIEK, K. A., BRIGGS, K. J., ROBBINS, A. K., SEWASTIANIK, T., SHAREEF, S. J., OLENCHOCK, B. A., PARKER, S. J., TATEISHI, K., SPINELLI, J. B., ISLAM, M., HAIGIS, M. C., LOOPER, R. E., LIGON, K. L., BERNSTEIN, B. E., CARRASCO, R. D., CAHILL, D. P., ASARA, J. M., METALLO, C. M., YENNAWAR, N. H., VANDER HEIDEN, M. G. & KAELIN, W. G., JR. 2018. Transaminase Inhibition by 2-Hydroxyglutarate Impairs Glutamate Biosynthesis and Redox Homeostasis in Glioma. *Cell,* 175**,** 101-116 e25.

NADTOCHIY, S. M., SCHAFER, X., FU, D., NEHRKE, K., MUNGER, J. & BROOKES, P. S. 2016. Acidic pH Is a Metabolic Switch for 2-Hydroxyglutarate Generation and Signaling. *J Biol Chem,* 291**,** 20188-97.

NAM, H., KUNDU, A., BRINKLEY, G. J., CHANDRASHEKAR, D. S., KIRKMAN, R. L., CHAKRAVARTHI, B., ORLANDELLA, R. M., NORIAN, L. A., SONPAVDE, G., GHATALIA, P., FEI, F., WEI, S., VARAMBALLY, S. & SUDARSHAN, S. 2020b. PGC1alpha suppresses kidney cancer progression by inhibiting collagen-induced SNAIL expression. *Matrix Biol,* 89**,** 43-58.

NIEMANN, S. & MULLER, U. 2000. Mutations in SDHC cause autosomal dominant paraganglioma, type 3. *Nat Genet,* 26**,** 268-70.

OLDHAM, W. M., CLISH, C. B., YANG, Y. & LOSCALZO, J. 2015. Hypoxia-Mediated Increases in L-2-hydroxyglutarate Coordinate the Metabolic Response to Reductive Stress. *Cell Metab,* 22**,** 291-303.

PAPANDREOU, I., CAIRNS, R. A., FONTANA, L., LIM, A. L. & DENKO, N. C. 2006. HIF-1 mediates adaptation to hypoxia by actively downregulating mitochondrial oxygen consumption. *Cell Metab,* 3**,** 187-97.

PARSONS, D. W., JONES, S., ZHANG, X., LIN, J. C., LEARY, R. J., ANGENENDT, P., MANKOO, P., CARTER, H., SIU, I. M., GALLIA, G. L., OLIVI, A., MCLENDON, R., RASHEED, B. A., KEIR, S., NIKOLSKAYA, T., NIKOLSKY, Y., BUSAM, D. A., TEKLEAB, H., DIAZ, L. A., JR., HARTIGAN, J., SMITH, D. R., STRAUSBERG, R. L., MARIE, S. K., SHINJO, S. M., YAN, H., RIGGINS, G. J., BIGNER, D. D., KARCHIN, R., PAPADOPOULOS, N., PARMIGIANI, G., VOGELSTEIN, B., VELCULESCU, V. E. & KINZLER, K. W. 2008. An integrated genomic analysis of human glioblastoma multiforme. *Science,* 321**,** 1807-12.

RAKHEJA, D., BORIACK, R. L., MITUI, M., KHOKHAR, S., HOLT, S. A. & KAPUR, P. 2011. Papillary thyroid carcinoma shows elevated levels of 2-hydroxyglutarate. *Tumour Biol,* 32**,** 325-33.

RZEM, R., ACHOURI, Y., MARBAIX, E., SCHAKMAN, O., WIAME, E., MARIE, S., GAILLY, P., VINCENT, M. F., VEIGA-DA-CUNHA, M. & VAN SCHAFTINGEN, E. 2015. A mouse model of L-2-hydroxyglutaric aciduria, a disorder of metabolite repair. *PLoS One,* 10**,** e0119540.

RZEM, R., VINCENT, M. F., VAN SCHAFTINGEN, E. & VEIGA-DA-CUNHA, M. 2007. L-2-hydroxyglutaric aciduria, a defect of metabolite repair. *J Inherit Metab Dis,* 30**,** 681-9.

SEAVER, S. M., HENRY, C. S. & HANSON, A. D. 2012. Frontiers in metabolic reconstruction and modeling of plant genomes. *J Exp Bot,* 63**,** 2247-58.

SHELAR, S., SHIM, E. H., BRINKLEY, G. J., KUNDU, A., CAROBBIO, F., POSTON, T., TAN, J., PAREKH, V., BENSON, D., CROSSMAN, D. K., BUCKHAULTS, P. J., RAKHEJA, D., KIRKMAN, R., SATO, Y., OGAWA, S., DUTTA, S., VELU, S. E., EMBERLEY, E., PAN, A., CHEN, J., HUANG, T., ABSHER, D., BECKER, A., KUNICK, C. & SUDARSHAN, S. 2018. Biochemical and Epigenetic Insights into L-2-Hydroxyglutarate, a Potential Therapeutic Target in Renal Cancer. *Clin Cancer Res,* 24**,** 6433-6446.

SHIM, E. H., LIVI, C. B., RAKHEJA, D., TAN, J., BENSON, D., PAREKH, V., KHO, E. Y., GHOSH, A. P., KIRKMAN, R., VELU, S., DUTTA, S., CHENNA, B., REA, S. L., MISHUR, R. J., LI, Q., JOHNSON-PAIS, T. L., GUO, L., BAE, S., WEI, S., BLOCK, K. & SUDARSHAN, S. 2014. L-2-Hydroxyglutarate: an epigenetic modifier and putative oncometabolite in renal cancer. *Cancer Discov,* 4**,** 1290-8.

SHIM, E. H. & SUDARSHAN, S. 2015. Another small molecule in the oncometabolite mix: L-2-Hydroxyglutarate in kidney cancer. *Oncoscience,* 2**,** 483-6.

SU, R., DONG, L., LI, C., NACHTERGAELE, S., WUNDERLICH, M., QING, Y., DENG, X., WANG, Y., WENG, X., HU, C., YU, M., SKIBBE, J., DAI, Q., ZOU, D., WU, T., YU, K., WENG, H., HUANG, H., FERCHEN, K., QIN, X., ZHANG, B., QI, J., SASAKI, A. T., PLAS, D. R., BRADNER, J. E., WEI, M., MARCUCCI, G., JIANG, X., MULLOY, J. C., JIN, J., HE, C. & CHEN, J. 2018. R-2HG Exhibits Anti-tumor Activity by Targeting FTO/m(6)A/MYC/CEBPA Signaling. *Cell,* 172**,** 90-105 e23.

TENG, X., EMMETT, M. J., LAZAR, M. A., GOLDBERG, E. & RABINOWITZ, J. D. 2016. Lactate Dehydrogenase C Produces S-2-Hydroxyglutarate in Mouse Testis. *ACS Chem Biol,* 11**,** 2420-7.

TOMLINSON, I. P., ALAM, N. A., ROWAN, A. J., BARCLAY, E., JAEGER, E. E., KELSELL, D., LEIGH, I., GORMAN, P., LAMLUM, H., RAHMAN, S., ROYLANCE, R. R., OLPIN, S., BEVAN, S., BARKER, K., HEARLE, N., HOULSTON, R. S., KIURU, M., LEHTONEN, R., KARHU, A., VILKKI, S., LAIHO, P., EKLUND, C., VIERIMAA, O., AITTOMAKI, K., HIETALA, M., SISTONEN, P., PAETAU, A., SALOVAARA, R., HERVA, R., LAUNONEN, V., AALTONEN, L. A. & MULTIPLE LEIOMYOMA, C. 2002. Germline mutations in FH predispose to dominantly inherited uterine fibroids, skin leiomyomata and papillary renal cell cancer. *Nat Genet,* 30**,** 406-10.

VAN DER KNAAP, M. S., JAKOBS, C., HOFFMANN, G. F., NYHAN, W. L., RENIER, W. O., SMEITINK, J. A., CATSMAN-BERREVOETS, C. E., HJALMARSON, O., VALLANCE, H., SUGITA, K., BOWE, C. M., HERRIN, J. T., CRAIGEN, W. J., BUIST, N. R., BROOKFIELD, D. S. & CHALMERS, R. A. 1999. D-2-Hydroxyglutaric aciduria: biochemical marker or clinical disease entity? *Ann Neurol,* 45**,** 111-9.

WANG, J., DUNCAN, D., SHI, Z. & ZHANG, B. 2013. WEB-based GEne SeT AnaLysis Toolkit (WebGestalt): update 2013. *Nucleic Acids Res,* 41**,** W77-83.

WANG, J., VASAIKAR, S., SHI, Z., GREER, M. & ZHANG, B. 2017. WebGestalt 2017: a more comprehensive, powerful, flexible and interactive gene set enrichment analysis toolkit. *Nucleic Acids Res,* 45**,** W130-W137.

WEBER, J. & RAD, R. 2019. Engineering CRISPR mouse models of cancer. *Curr Opin Genet Dev,* 54**,** 88-96.

WETTERSTEN, H. I. 2020. Reprogramming of Metabolism in Kidney Cancer. *Semin Nephrol,* 40**,** 2-13.

XU, W., YANG, H., LIU, Y., YANG, Y., WANG, P., KIM, S. H., ITO, S., YANG, C., WANG, P., XIAO, M. T., LIU, L. X., JIANG, W. Q., LIU, J., ZHANG, J. Y., WANG, B., FRYE, S., ZHANG, Y., XU, Y. H., LEI, Q. Y., GUAN, K. L., ZHAO, S. M. &

XIONG, Y. 2011. Oncometabolite 2-hydroxyglutarate is a competitive inhibitor of alpha-ketoglutarate-dependent dioxygenases. *Cancer Cell,* 19**,** 17-30.

YAN, H., PARSONS, D. W., JIN, G., MCLENDON, R., RASHEED, B. A., YUAN, W., KOS, I., BATINIC-HABERLE, I., JONES, S., RIGGINS, G. J., FRIEDMAN, H., FRIEDMAN, A., REARDON, D., HERNDON, J., KINZLER, K. W., VELCULESCU, V. E., VOGELSTEIN, B. & BIGNER, D. D. 2009. IDH1 and IDH2 mutations in gliomas. *N Engl J Med,* 360**,** 765-73.

ZHANG, B., KIROV, S. & SNODDY, J. 2005. WebGestalt: an integrated system for exploring gene sets in various biological contexts. *Nucleic Acids Res,* 33**,** W741-8.

Figures

A

wt	GTGGCTGGGGGCTTCCTCCGCGCAAGTGGACCGGCGTCCGGGGTGCCCGGGCTA	
	-V--A--G--G--F--L--R--A--S--G--P--A--S--G--V--P--G--L-	
mut	GTGGCTGGGGGC----------AAGTGGACCGGCGTCCGGGGTGCCCGGGCTA	-11 bp
	-V--A--G--G----------K--W--T--G--V--R--G--A--R--A--	Frameshift
	(22 wt aa, 24 fs aa & Stop)	

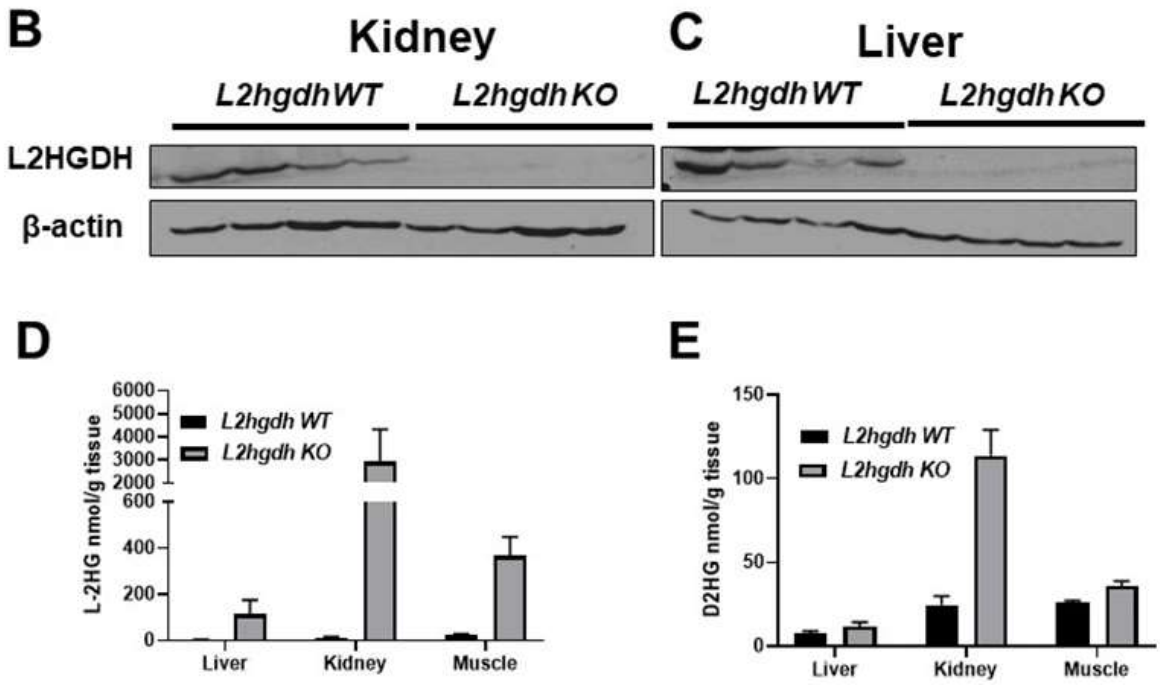

Figure 1. CRISPR/Cas9 knockout of *L2hghd* increases L-2HG levels. A) *L2hgdh* sequence of mouse wild type (WT) and mutant (KO) allele generated demonstrating 11 base pair deletion with resulting frameshift (fs) and premature stop codon. Yellow highlighted region indicates target PAM sequence. B, C) Immunoblot for L2HGDH and actin of both liver and kidney tissue from *L2hgdh WT* and *KO* mice D, E) GC/MS measurements of L- and D- 2-HG in liver, kidney, and muscle tissues. Mice fasted for 12 hours prior to initial tissue harvest. Data represent means +/- s.e.m.

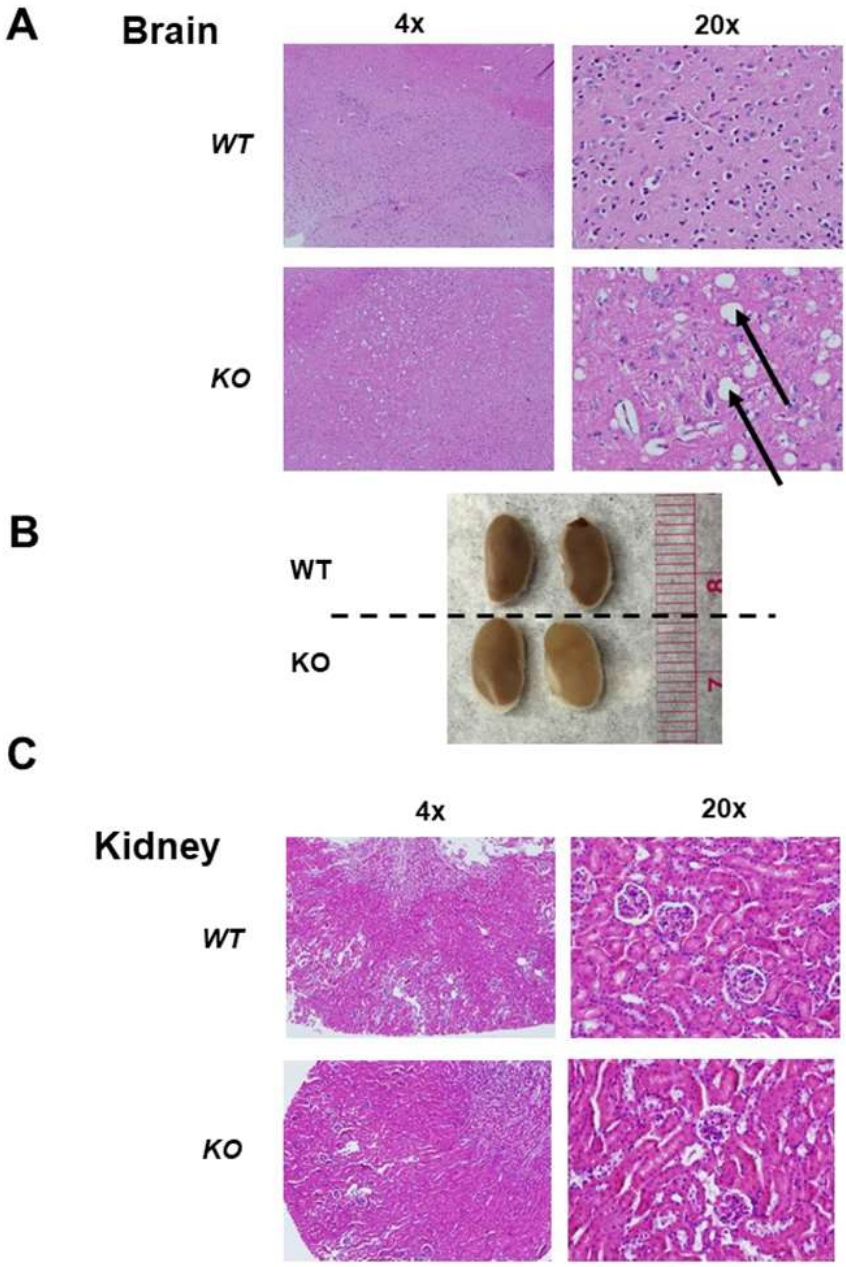

Figure 2. Histological analysis of L2hgdh WT(+/+) and KO (-/-) tissues. A) Slices of mouse cerebral cortex stained with H&E. Vacuoles (indicated by black arrows) are noted in L2hgdh KO. B) Gross images of kidneys from WT and KO animals. C) Slices of mouse kidney cortex stained with H&E. Normal appearing glomeruli and proximal tubules can be identified in both WT and KO. Images displayed show 4x and 20x magnification.

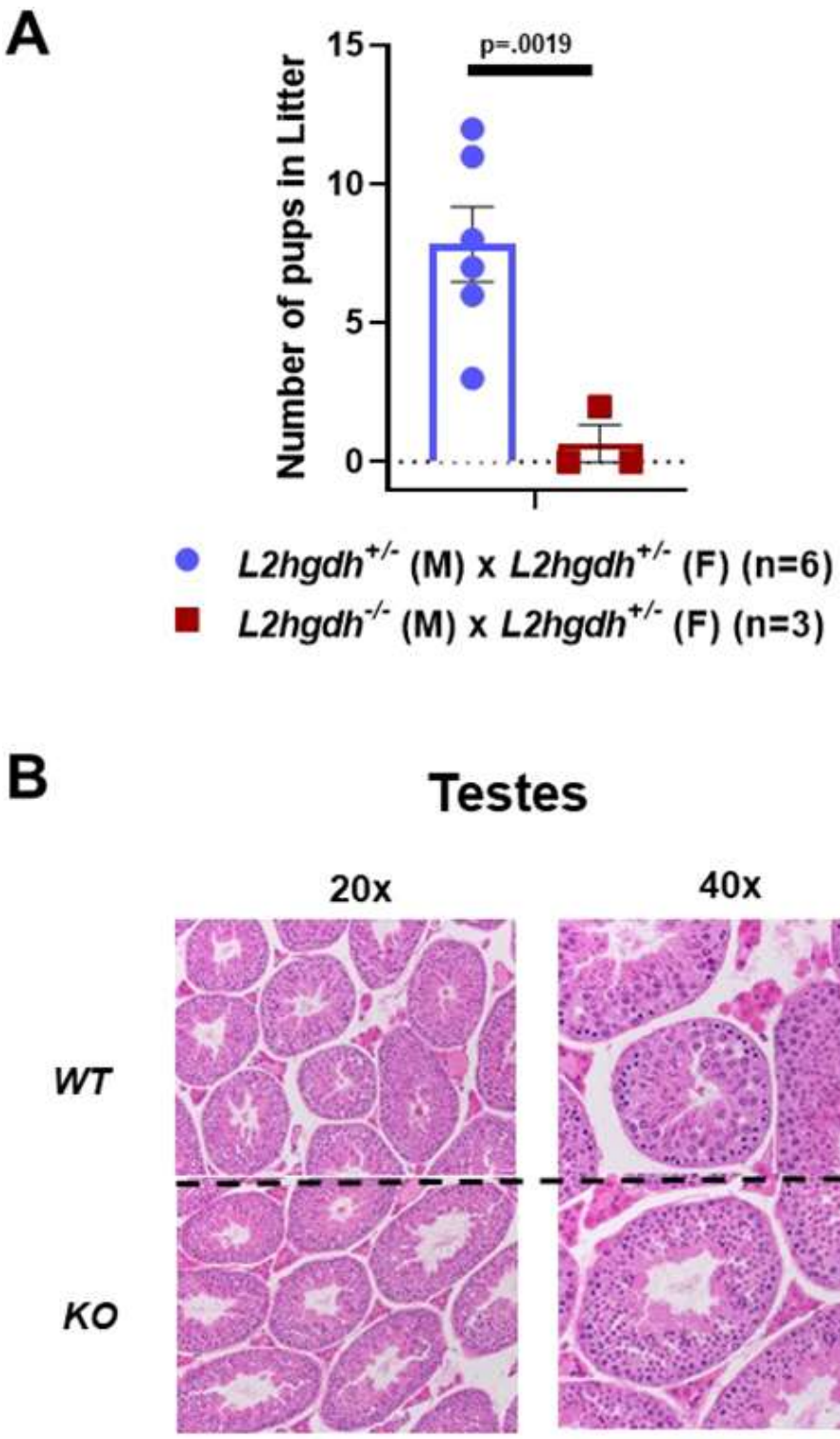

Figure 3. Fertility analysis of *L2hgdh* heterozygous (+/-) and KO male mice. A) Number of pups per liter generated when crossing a heterozygous female (+/-) with either a heterozygous male (+/-) (blue) or homozygous null (-/-) male (red). n= number of breeding pairs examined. Graph denotes 2-tailed t-test result and means +/- s.e.m. B) Slices of mouse testes after Bouin's fixation and staining with H&E. Images displayed show 20x and 40x magnification.

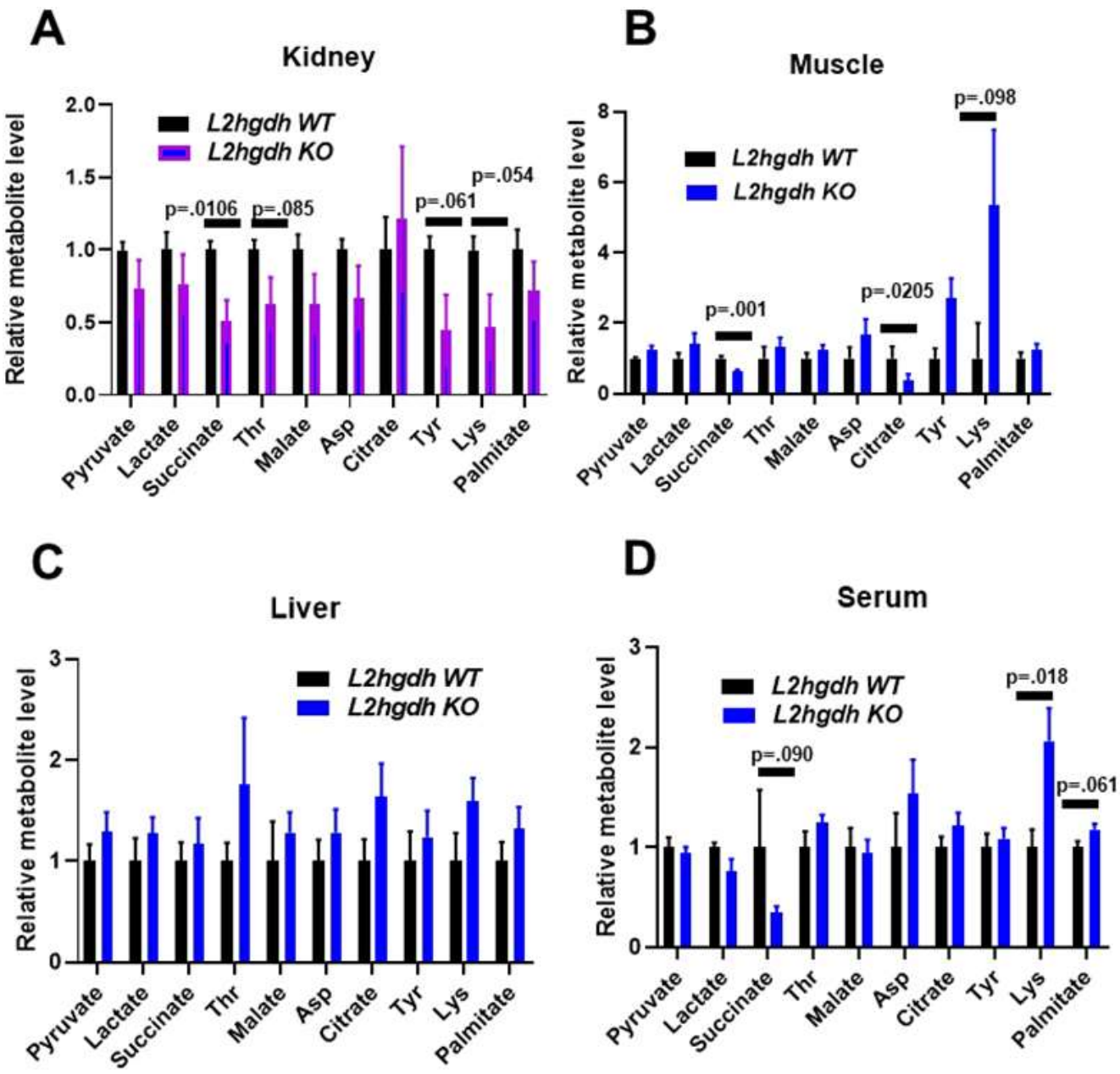

Figure 4. Metabolite profiling of WT and KO tissues. GC-MS metabolite profiling of tissues and serum from *WT* and *KO* mice. Mice were fasted for 12 hours prior to sample harvest and metabolite extraction. Values are normalized to *L2hgdh WT* metabolite amount. n=5 mice for each group. Both groups contain both male and female mice. Graphs depict 2-tailed t-tests and means +/- s.e.m.

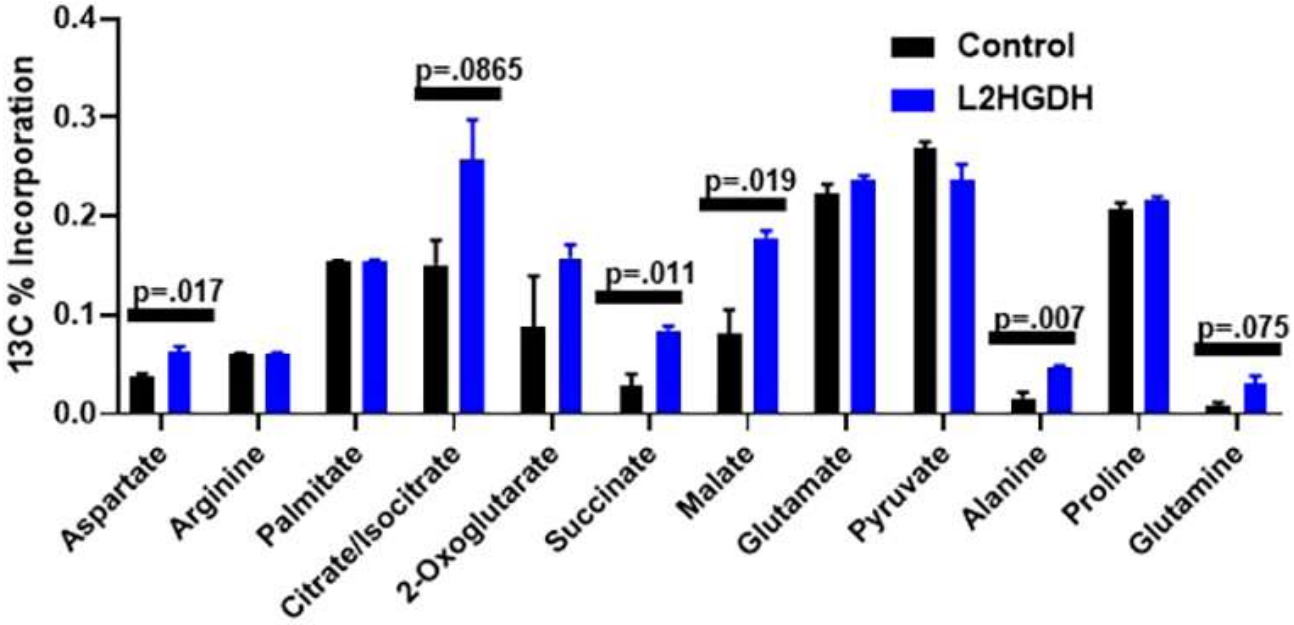

Figure 5. Metabolite flux analysis of 769-P RCC cells +/- L2HGDH incubated with [U-13C] glucose. 769-P RCC cells were stably transduced with control vector or L2HGDH. Cells were then treated with [U-^{13}C] glucose for 24 hours followed by metabolite extraction and LC/MS profiling. Values represent total 13C label incorporation into the indicated metabolite. Graph depicts 2-tailed t-tests and means +/- s.e.m.

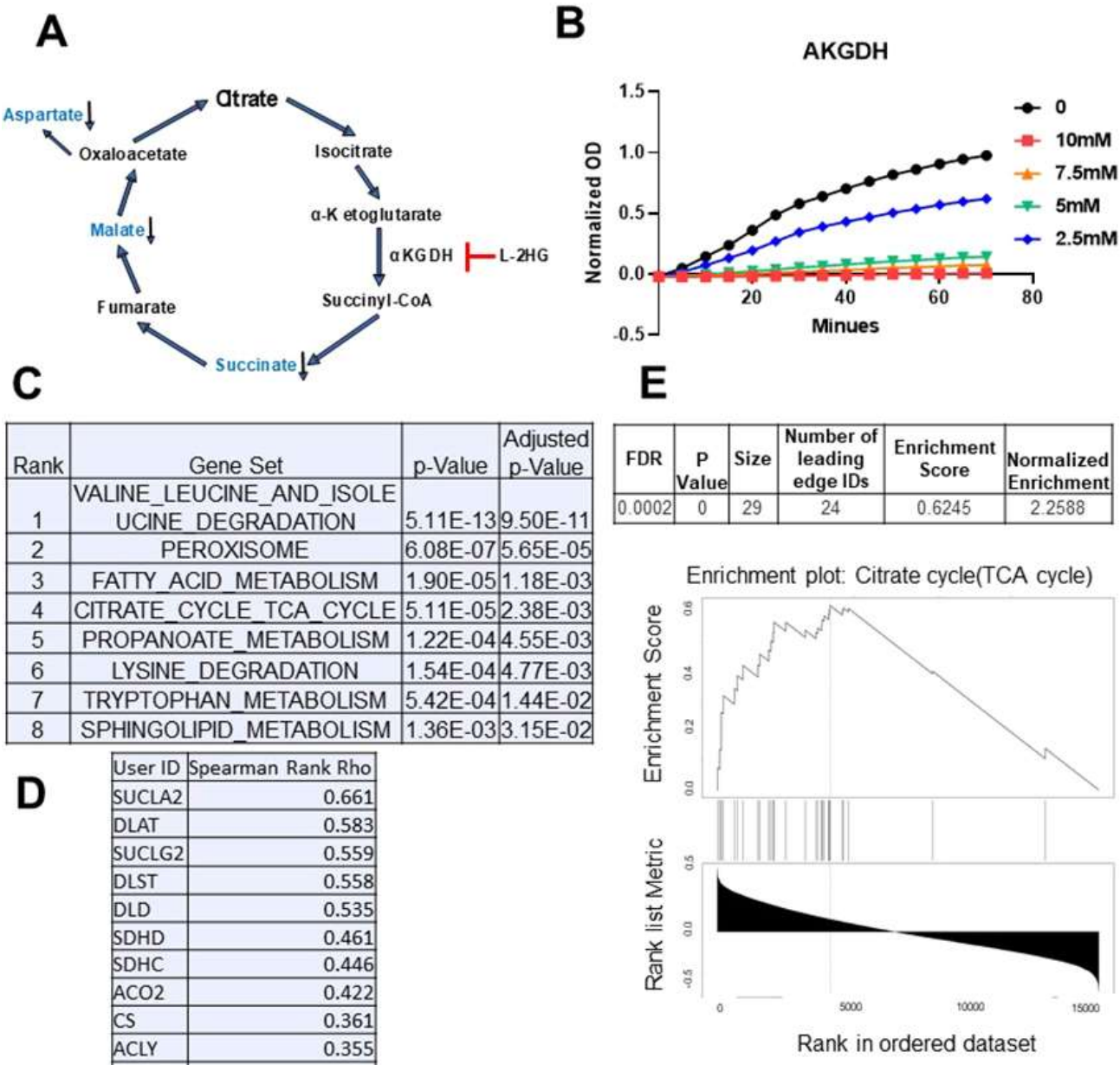

C

Rank	Gene Set	p-Value	Adjusted p-Value
1	VALINE_LEUCINE_AND_ISOLEUCINE_DEGRADATION	5.11E-13	9.50E-11
2	PEROXISOME	6.08E-07	5.65E-05
3	FATTY_ACID_METABOLISM	1.90E-05	1.18E-03
4	CITRATE_CYCLE_TCA_CYCLE	5.11E-05	2.38E-03
5	PROPANOATE_METABOLISM	1.22E-04	4.55E-03
6	LYSINE_DEGRADATION	1.54E-04	4.77E-03
7	TRYPTOPHAN_METABOLISM	5.42E-04	1.44E-02
8	SPHINGOLIPID_METABOLISM	1.36E-03	3.15E-02

D

User ID	Spearman Rank Rho
SUCLA2	0.661
DLAT	0.583
SUCLG2	0.559
DLST	0.558
DLD	0.535
SDHD	0.461
SDHC	0.446
ACO2	0.422
CS	0.361
ACLY	0.355
OGDH	0.324
OGDHL	0.316
PCK1	0.307
ACO1	0.305

E

FDR	P Value	Size	Number of leading edge IDs	Enrichment Score	Normalized Enrichment
0.0002	0	29	24	0.6245	2.2588

Figure 6. The L-2HG/ L2HGDH axis and the TCA cycle. A) Schematic of L-2HG's proposed effects on TCA cycle based on flux analysis. B) Effects of increasing L-2HG levels on α-KGDH enzymatic activity in vitro. α-KGDH enzymatic product formation was measured based on optical density at 450nm. C) KEGG (https://www.genome.jp/kegg/) pathway analysis of L2HGDH positively correlated genes in clear cell RCC with Spearman Rank >.3 (moderate association). Co-expression analysis performed by GRACE (https://grace.biohpc.swmed.edu/). Pathway analysis performed by Enrichr (https://amp.pharm.mssm.edu/Enrichr/). Data from TCGA KIRC data set. D) TCA cycle genes positively correlated with L2HGDH from KEGG TCA cycle pathway utilized in C.

E) Enrichment plot of KEGG TCA cycle using all genes from KIRC L2HGDH GRACE analysis. Analysis performed by Webgesalt (http://www.webgestalt.org/) utilizing Spearman Rank Rho for rank order.

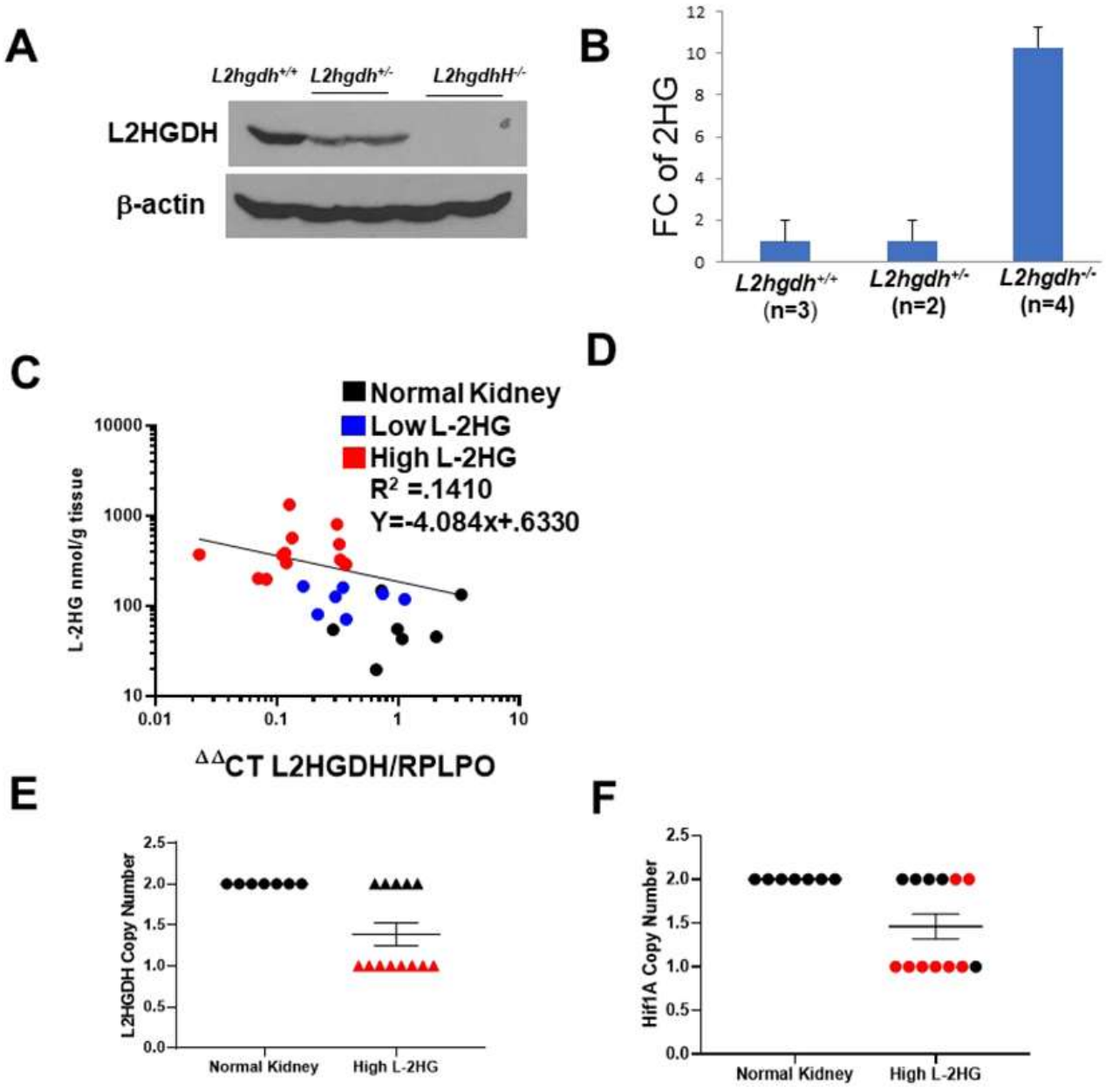

Figure 7. Alternative mechanisms contribute to decreased *L2HGDH* mRNA in kidney cancerA) Immunoblot of L2HGDH in kidneys from *L2hgdh*$^{+/+}$, *L2hgdh*$^{+/-}$, and *L2hgdh*$^{-/-}$ mice. B) Renal 2HG (normalized) from mice with the indicated genotype. C) *L2HGDH* mRNA (x-axis) and L-2HG metabolite levels (y-axis) in RCC tumors and normal kidney (black). RCC tumor samples were designated either low L-2HG (blue) or high L-2HG (red). Low L-2HG designation is based on metabolite level within 2 standard deviations away from normal kidney median L-2HG levels. Correlation line created in Graphpad Prism 8 using Log-Log line non-linear fit. E and F) Copy number analysis by qPCR for *L2HGDH* and *HIF1A* in normal kidney and high L-2HG renal tumors. Both genes are located on 14q. Red values depict tumors with copy loss for *L2HGDH*.

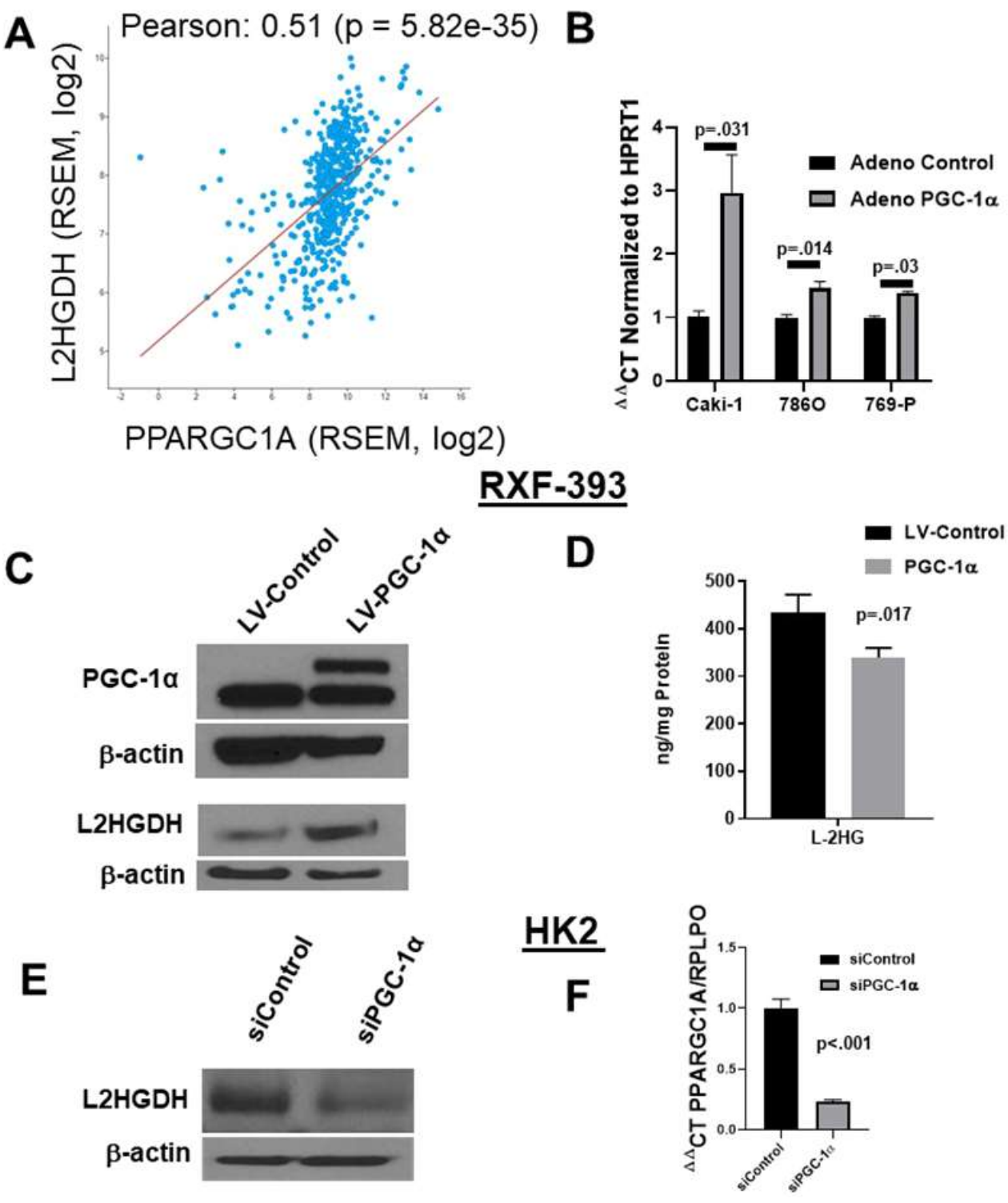

Figure 8. PGC-1α regulates L2HGDH expression. A) TCGA KIRC (clear cell RCC) correlation plot comparing RSEM RNA values for *PPARGC1A* and *L2HGDH* using cBIO analysis portal (http://www.cbioportal.org/). B) *L2HGDH* mRNA expression was assessed in RCC lines following adenoviral delivery of PGC-1α relative to control adenovirus. C) Immunoblot analysis for L2HGDH following stable lentiviral (LV) expression of PGC-1α in

RXF-393 RCC cells. For PGC1-α immunoblot, lower band represents nonspecific band. D) L-2HG levels in RXF-393 cells +/- PGC-1α. E) Immunoblot for L2HGDH in HK2 renal epithelial cells following transfection with the indicated siRNA. E) RT-qPCR for *PPARGC1A* following treatment with the indicated siRNA in HK2 cells. Graphs depict 2-tailed t-tests and means +/- s.e.m.

A

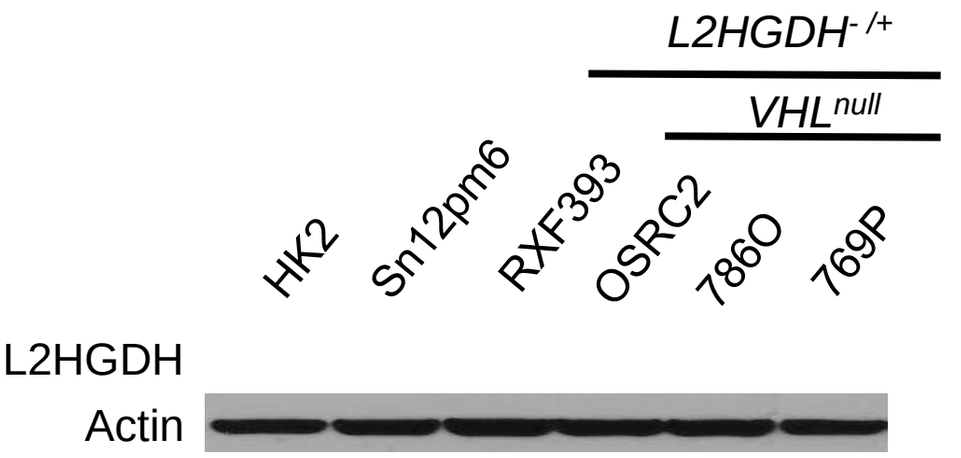

B

Cell line	14q-Status	VHL-status	L2HGDH-CNV	Hif1a-CNV	Dataset	Sources
HEK293T	WT	WT	0	0		(Lin et al., 2014)
HK2	WT	WT	0	0		(Brodaczewska, Szczylik, Fiedorowicz, Porta, & Czarnecka, 2016) (Tym et al., 2016)
Sn12pm6	No Data	No Data	No Data	No Data		
RXF393	No Data	WT	-1	0	NCI-60	(Reinhold et al., 2012) (Suwaki et al., 2011)
OSRC2	No Data	Mutant	-1	1	Cancer Cell Line Encyclopedia 2012	(Barretina et al., 2012) (Reinhold et al., 2012)
786O	Loss	Mutant	-1	-2	Cancer Cell Line Encyclopedia 2012	(Alimov et al., 2000) (Barretina et al., 2012) (Brodaczewska, Szczylik, Fiedorowicz, Porta, & Czarnecka, 2016) (Strefford et al., 2005)
769P	Loss	Mutant	-1	-2	Cancer Cell Line Encyclopedia 2012	(Alimov et al., 2000) (Barretina et al., 2012) (Brodaczewska, Szczylik, Fiedorowicz, Porta, & Czarnecka, 2016) (Strefford et al., 2005)
Caki1	Loss	WT	-1	-1	Cancer Cell Line Encyclopedia 2012	(Alimov et al., 2000) (Barretina et al., 2012) (Brodaczewska, Szczylik, Fiedorowicz, Porta, & Czarnecka, 2016) (Strefford et al., 2005)

Figure S1. RCC cell line description. A) Immunoblot for L2HGDH in various cell lines. Genomic *L2HGDH* and *VHL* status depicted. Sn12pm6 L2HGDH status is unknown but believed to be homozygous WT and VHL. **B)** Table characterizing Cell lines used. Dataset indicated in cbioportal (https://www.cbioportal.org/) analysis displayed in fifth column. CNV refers to copy number variants. Negative values depict copy loss of gene, and positive numbers depict copy gain of gene.

Alimov, A., Kost-Alimova, M., Liu, J., Li, C., Bergerheim, U., Imreh, S., . . . Zabarovsky, E. R. (2000). Combined LOH/CGH analysis proves the existence of interstitial 3p deletions in renal cell carcinoma. *Oncogene, 19*(11), 1392-1399. doi:10.1038/sj.onc.1203449

Barretina, J., Caponigro, G., Stransky, N., Venkatesan, K., Margolin, A. A., Kim, S., . . . Garraway, L. A. (2012). The Cancer Cell Line Encyclopedia enables predictive modelling of anticancer drug sensitivity. *Nature, 483*(7391), 603-607. doi:10.1038/nature11003

Brodaczewska, K. K., Szczylik, C., Fiedorowicz, M., Porta, C., & Czarnecka, A. M. (2016). Choosing the right cell line for renal cell cancer research. *Mol Cancer, 15*(1), 83. doi:10.1186/s12943-016-0565-8

Lin, Y. C., Boone, M., Meuris, L., Lemmens, I., Van Roy, N., Soete, A., . . . Callewaert, N. (2014). Genome dynamics of the human embryonic kidney 293 lineage in response to cell biology manipulations. *Nat Commun, 5*, 4767. doi:10.1038/ncomms5767

Reinhold, W. C., Sunshine, M., Liu, H., Varma, S., Kohn, K. W., Morris, J., . . . Pommier, Y. (2012). CellMiner: a web-based suite of genomic and pharmacologic tools to explore transcript and drug patterns in the NCI-60 cell line set. *Cancer Res, 72*(14), 3499-3511. doi:10.1158/0008-5472.CAN-12-1370

Strefford, J. C., Stasevich, I., Lane, T. M., Lu, Y. J., Oliver, T., & Young, B. D. (2005). A combination of molecular cytogenetic analyses reveals complex genetic alterations in conventional renal cell carcinoma. *Cancer Genet Cytogenet, 159*(1), 1-9. doi:10.1016/j.cancergencyto.2004.09.020

Suwaki, N., Vanhecke, E., Atkins, K. M., Graf, M., Swabey, K., Huang, P., . . . Thomas, G. V. (2011). A HIF-regulated VHL-PTP1B-Src signaling axis identifies a therapeutic target in renal cell carcinoma. *Sci Transl Med, 3*(85), 85ra47. doi:10.1126/scitranslmed.3002004

Tym, J. E., Mitsopoulos, C., Coker, E. A., Razaz, P., Schierz, A. C., Antolin, A. A., & Al-Lazikani, B. (2016). canSAR: an updated cancer research and drug discovery knowledgebase. *Nucleic Acids Res, 44*(D1), D938-943. doi:10.1093/nar/gkv1030

A

	Kidney	Kidney	Liver	Liver	Muscle	Muscle
	L2HG nM/g tissue	D2HG nM/g tissue	L2HG nM/g tissue	D2HG nM/g tissue	L2HG nM/g tissue	D2HG nM/g tissue
WT	10.82170153	33.57294421	1.205087373	2.88015882	24.06087393	28.84996874
WT	3.015182025	6.083730104	1.066566642	1.947983574	17.46666102	27.4105522
WT	7.594435277	21.12633813	2.147866761	7.041052875	12.3863429	21.06340664
WT	12.12458138	43.60550698	3.323879612	10.40413194	18.63936778	27.07146272
WT	12.77616118	25.94254448	5.738375694	14.30179788	21.18718248	28.76073958
HET	17.61376121	17.4397504	2.762264261	7.512958099	34.3930556	20.5975885
KO	4995.348645	129.6887608	227.2257509	23.27037387	376.7103529	31.45932202
KO	2935.883314	127.9893919	42.69314487	4.649831253	201.1203439	34.01738755
KO	1323.109679	75.91966485	106.9425919	12.63449326	382.2049692	34.3988449
KO	4135.785813	175.3279618	101.261952	7.433704276	388.2907435	35.97909948
KO	1873.173888	80.71231653	120.4738564	12.04866266	423.2089644	49.10728638
KO	2303.892806	91.60806449	79.00750239	9.937049517	422.4779693	31.41682567

Figure S2. L-2HG measurement values from KO mice and littermate controls. A) L-2HG measurements by GC/MS. Mouse Genotype depicted as *L2hgdh*$^{+/+}$ (WT), *L2hgdh*$^{+/-}$ (Het), and *L2hgdh*$^{-/-}$ (KO). As described in methods, mice were fasted for 12 hours prior to metabolite extraction. Het mice demonstrated similar L-2HG measurements as WT in all tissues. Values color coordinated based on value with red = higher and blue = lesser values of 2HG.

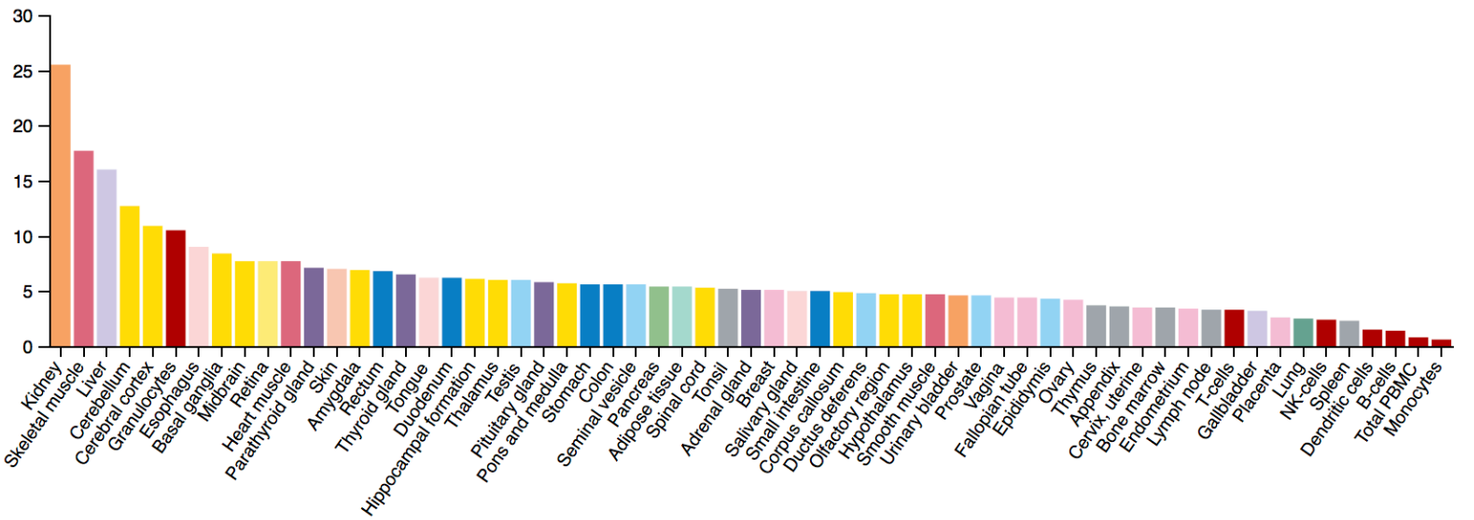

Figure S3. Consensus tissue expression of L2HGDH from three transcriptomic data sets (Human Protein Atlas RNAseq data, GTEx, and CAGE data from the FANTOM5 project) (https://www.proteinatlas.org/ENSG00000087299-L2HGDH/tissue).

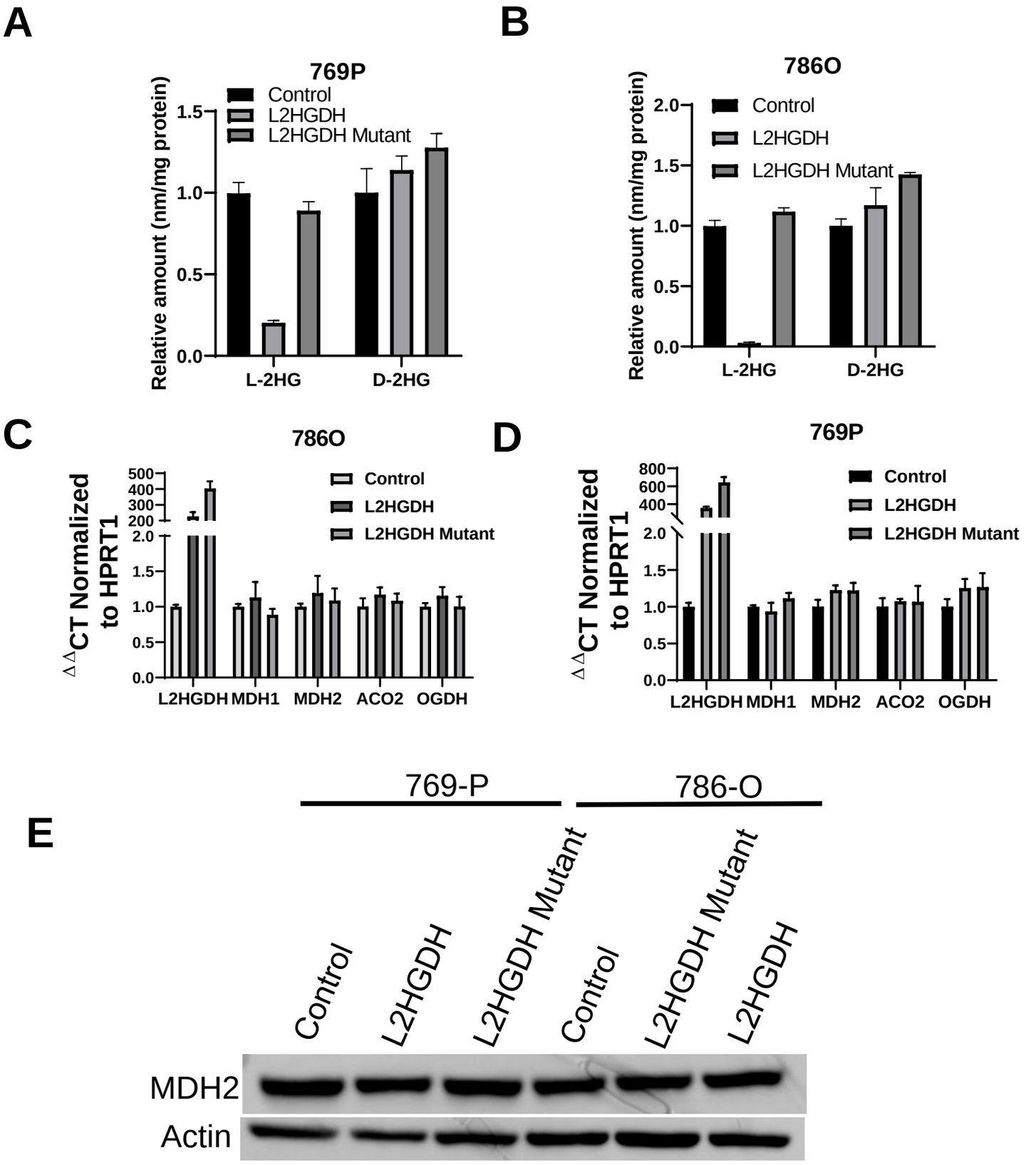

Figure S4. L-2HG does not impact TCA cycle enzyme levels. A, B) D/L- 2HG levels in 769-P and 786O RCC cells expressing control vector , WT L2HGDH, and mutant A241G L2HGDH. Cells were then analyzed for relative mRNA (panels C,D) and protein (panel E) expression of TCA cycle enzymes.

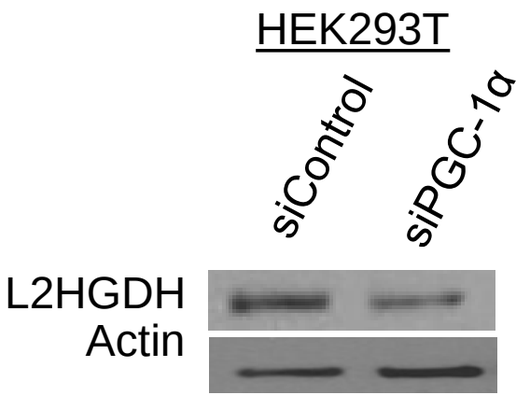

Figure S5. PGC-1α knockdown in HEK293T. Immunoblot of embryonic kidney cell line HEK293T cells with both siControl and siPGC-1α knockdown depicting L2HGDH and actin levels.

Table S1

Click here to Download Table S1

Table S2

Click here to Download Table S2

Table S3

Click here to Download Table S3